AERO. & ASTRO. LIBRARY

MASS. INST. TECH. AERO. ENG. LIBRARY

NATIONAL ADVISORY COMMITTEE FOR AERONAUTICS

REPORT No. 875

Copy #3

APPLICATION OF THE ANALOGY BETWEEN WATER FLOW WITH A FREE SURFACE AND TWO-DIMENSIONAL COMPRESSIBLE GAS FLOW

By W. JAMES ORLIN, NORMAN J. LINDNER, and JACK G. BITTERLY



1947

For sale by the Superintendent of Documents, U. S. Government Printing Office, Washington 25, D. C. - - - - - - - - - - Price 15 cents

623.742
U58

AERONAUTIC SYMBOLS

1. FUNDAMENTAL AND DERIVED UNITS

	Symbol	Metric		English	
		Unit	Abbreviation	Unit	Abbreviation
Length	l	meter	m	foot (or mile)	ft (or mi)
Time	t	second	s	second (or hour)	sec (or hr)
Force	F	weight of 1 kilogram	kg	weight of 1 pound	lb
Power	P	horsepower (metric)		horsepower	hp
Speed	V	kilometers per hour	kph	miles per hour	mph
		meters per second	mps	feet per second	fps

2. GENERAL SYMBOLS

W Weight $= mg$

g Standard acceleration of gravity $= 9.80665$ m/s^2 or 32.1740 ft/sec^2

m Mass $= \frac{W}{g}$

I Moment of inertia $= mk^2$. (Indicate axis of radius of gyration k by proper subscript.)

μ Coefficient of viscosity

ν Kinematic viscosity

ρ Density (mass per unit volume)

Standard density of dry air, 0.12497 kg-m^{-4}-s^2 at 15° C and 760 mm; or 0.002378 lb-ft^{-4} sec^2

Specific weight of "standard" air, 1.2255 kg/m^3 or 0.07651 lb/cu ft

3. AERODYNAMIC SYMBOLS

S Area

S_w Area of wing

G Gap

b Span

c Chord

A Aspect ratio, $\frac{b^2}{S}$

V True air speed

q Dynamic pressure, $\frac{1}{2}\rho V^2$

L Lift, absolute coefficient $C_L = \frac{L}{qS}$

D Drag, absolute coefficient $C_D = \frac{D}{qS}$

D_0 Profile drag, absolute coefficient $C_{D_0} = \frac{D_0}{qS}$

D_i Induced drag, absolute coefficient $C_{D_i} = \frac{D_i}{qS}$

D_p Parasite drag, absolute coefficient $C_{Dp} = \frac{D_p}{qS}$

C Cross-wind force, absolute coefficient $C_C = \frac{C}{qS}$

i_w Angle of setting of wings (relative to thrust line)

i_t Angle of stabilizer setting (relative to thrust line)

Q Resultant moment

Ω Resultant angular velocity

R Reynolds number, $\rho\frac{Vl}{\mu}$ where l is a linear dimension (e.g., for an airfoil of 1.0 ft chord, 100 mph, standard pressure at 15° C, the corresponding Reynolds number is 935,400; or for an airfoil of 1.0 m chord, 100 mps, the corresponding Reynolds number is 6,865,000)

α Angle of attack

ϵ Angle of downwash

α_o Angle of attack, infinite aspect ratio

α_i Angle of attack, induced

α_a Angle of attack, absolute (measured from zero-lift position)

γ Flight-path angle

REPORT No. 875

APPLICATION OF THE ANALOGY BETWEEN WATER FLOW WITH A FREE SURFACE AND TWO-DIMENSIONAL COMPRESSIBLE GAS FLOW

By W. JAMES ORLIN, NORMAN J. LINDNER, and JACK G. BITTERLY

Langley Memorial Aeronautical Laboratory
Langley Field, Va.

National Advisory Committee for Aeronautics

Headquarters, 1724 F Street NW, Washington 25, D. C.

Created by act of Congress approved March 3, 1915, for the supervision and direction of the scientific study of the problems of flight (U. S. Code, title 49, sec. 241). Its membership was increased to 15 by act approved March 2, 1929. The members are appointed by the President, and serve as such without compensation.

JEROME C. HUNSAKER, Sc. D., Cambridge, Mass., *Chairman*

ALEXANDER WETMORE, Sc. D., Secretary, Smithsonian Institution, *Vice Chairman*

HON. JOHN R. ALISON, Assistant Secretary of Commerce.

VANNEVAR BUSH, Sc. D., Chairman, Research and Development Board, Department of National Defense.

EDWARD U. CONDON, PH. D., Director, National Bureau of Standards.

DONALD B. DUNCAN, Vice Admiral, Deputy Chief of Naval Operations (Air).

R. M. HAZEN, B. S., Chief Engineer, Allison Division, General Motors Corp.

WILLIAM LITTLEWOOD, M. E., Vice President, Engineering, American Airlines System.

THEODORE C. LONNQUEST, Rear Admiral, Assistant Chief for Research and Development, Bureau of Aeronautics, Navy Department.

EDWARD M. POWERS, Major General, United States Air Force, Deputy Chief of Staff, Matériel.

ARTHUR E. RAYMOND, M. S., Vice President, Engineering, Douglas Aircraft Co.

FRANCIS W. REICHELDERFER, Sc. D., Chief, United States Weather Bureau.

CARL SPAATZ, General, Chief of Staff, United States Air Force.

ORVILLE WRIGHT, Sc. D., Dayton, Ohio.

THEODORE P. WRIGHT, Sc. D., Administrator of Civil Aeronautics, Department of Commerce.

HUGH L. DRYDEN, PH. D., *Director of Aeronautical Research*

JOHN W. CROWLEY, JR., B. S., *Associate Director of Aeronautical Research*

JOHN F. VICTORY, LLM., *Executive Secretary*

E. H. CHAMBERLIN, *Executive Officer*

HENRY J. E. REID, Sc. D., Director, Langley Memorial Aeronautical Laboratory, Langley Field, Va.

SMITH J. DEFRANCE, B. S., Director Ames Aeronautical Laboratory, Moffett Field, Calif.

EDWARD R. SHARP, LL. B., Director, Flight Propulsion Research Laboratory, Cleveland Airport, Cleveland, Ohio

TECHNICAL COMMITTEES

AERODYNAMICS
POWER PLANTS FOR AIRCRAFT
AIRCRAFT CONSTRUCTION
OPERATING PROBLEMS
SELF-PROPELLED GUIDED MISSILES
INDUSTRY CONSULTING

Coordination of Research Needs of Military and Civil Aviation
Preparation of Research Programs
Allocation of Problems
Prevention of Duplication
Consideration of Inventions

LANGLEY MEMORIAL AERONAUTICAL LABORATORY,
Langley Field, Va.

AMES AERONAUTICAL LABORATORY,
Moffett Field, Calif.

FLIGHT PROPULSION RESEARCH LABORATORY,
Cleveland Airport, Cleveland, Ohio

Conduct, under unified control, for all agencies, of scientific research on the fundamental problems of flight

OFFICE OF AERONAUTICAL INTELLIGENCE,
Washington, D. C.

Collection, classification, compilation, and dissemination of scientific and technical information on aeronautics

REPORT No. 875

APPLICATION OF THE ANALOGY BETWEEN WATER FLOW WITH A FREE SURFACE AND TWO-DIMENSIONAL COMPRESSIBLE GAS FLOW

By W. James Orlin, Norman J. Lindner, and Jack G. Bitterly

SUMMARY

The theory of the hydraulic analogy—that is, the analogy between water flow with a free surface and two-dimensional compressible gas flow—and the limitations and conditions of the analogy are discussed. A test was run using the hydraulic analogy as applied to the flow about circular cylinders of various diameters at subsonic velocities extending into the supercritical range. The apparatus and techniques used in this application are described and criticized. Reasonably satisfactory agreement of pressure distributions and flow fields existed between water and air flow about corresponding bodies. This agreement indicated the possibility of extending experimental compressibility research by new methods.

INTRODUCTION

An analogy exists between water flow with a free surface and two-dimensional compressible gas flow (hydraulic analogy). The water must flow over a smooth horizontal surface bounded by vertical walls geometrically similar to the walls bounding the corresponding compressible gas flow.

The mathematical basis of this hydraulic analogy was presented by Riabouchinsky in reference 1, in which he also described his apparatus for investigating the flow in a Laval nozzle. In reference 2, he extended the theory to include drag considerations and outlined the probable usefulness of the hydraulic analogy. Binnie and Hooker, in reference 3, obtained surveys along the center line of a channel with a constriction. By employing the characteristics method to calculate accurately the flow in a Laval nozzle, Preiswerk, in reference 4, demonstrated conclusively that the methods of gas dynamics can be applied to water flow with a free surface.

The National Advisory Committee for Aeronautics became interested in the hydraulic analogy because it seemed an easy and inexpensive way of studying two-dimensional compressible gas flow; in particular, phenomena occurring in air at speeds too high for visual observations could be observed at very low speeds (3 or 4 fps) in a water channel. Preliminary investigations were made in the Langley tank no. 1, where difficulty with the vertical accelerations—assumed negligibly small in the analogy—was experienced.

A water channel was designed and constructed in the Langley 8-foot high-speed tunnel in the spring of 1940. The channel was so constructed that flow fields involving both subsonic and supersonic velocities about aerodynamic bodies could be investigated. The value of the analogy in such flow fields has not been previously demonstrated. The development of the measuring apparatus and techniques is presented herein. The application of the analogy to flows through nozzles and about circular cylinders at subsonic velocities extending into the supercritical range is also presented.

SYMBOLS

c_p	specific heat at constant pressure
c_v	specific heat at constant volume
γ	adiabatic gas constant, ratio of c_p to c_v of gas
T	absolute temperature of gas
ρ	mass density of gas
p	pressure of gas
h	enthalpy or total heat content
q	dynamic pressure of gas $\left(\frac{1}{2}\rho V^2\right)$
σ	surface tension of liquid
P	pressure coefficient $\left(\frac{p_l - p_s}{q}\right)$
μ	viscosity of liquid
a	speed of sound in gas $\left(\sqrt{\gamma \frac{p}{\rho}}\right)$
V	velocity of flow
d	water depth
M	Mach number, stream value unless otherwise indicated (V/a for gas; $V/\sqrt{gd}$ for water)
g	acceleration of gravity
F_c	compressibility factor
x, y	rectangular coordinate axes
u, v	components of velocity in x-direction and y-direction, respectively
ϕ	velocity potential in two-dimensional flow
λ	wave length of surface waves in fluid
U	velocity of propagation of surface waves in fluid
D	diameter of circular cylinder
R	Reynolds number ($VD\rho/\mu$)
θ	angular measurement clockwise about cylinder; at stagnation point, $\theta=0°$

Subscripts:

No subscript	any value of variable
0	value at stagnation ($V=0$)
st	value for completely undisturbed static conditions, no flow in channel
l	local value of variable; value at surface of model, at channel walls, or in field of flow
s	value in undisturbed stream
1, 2	any two values of variable
max	maximum value of variable
cr	critical value of variable, value at which Mach number of 1 is reached at some point in flow
x	partial derivative with respect to x $\left(\text{for example: } \phi_x=\frac{\partial\phi}{\partial x};\ \phi_{xx}=\frac{\partial^2\phi}{\partial x^2}\right)$
y	partial derivative with respect to y

THEORY

The following is a condensation of the theory and mathematical development of the hydraulic analogy as given by Preiswerk (reference 4).

Two assumptions are made in the mathematical development:

(1) The flow is irrotational.

(2) The vertical accelerations at the free surface are negligible compared with the acceleration of gravity. The pressure in the fluid at any point therefore depends only on the height of the free surface above that point.

The analogy between the flow of water with free surface and the flow of a compressible gas may be obtained by setting up the energy equations for each. From the energy equation for water, the velocity is

$$V^2=2g(d_0-d) \tag{1a}$$

and

$$V_{max}=\sqrt{2gd_0} \tag{1b}$$

The corresponding equations for the velocity of a gas are

$$V^2=2g(h_0-h)=2gc_p(T_0-T) \tag{2a}$$

and

$$V_{max}=\sqrt{2gh_0}=\sqrt{2gc_pT_0} \tag{2b}$$

Therefore, if the ratio V/V_{max} for gas is equated to V/V_{max} for water,

$$\frac{d_0-d}{d_0}=\frac{h_0-h}{h_0}=\frac{T_0-T}{T_0}$$

or

$$\frac{d}{d_0}=\frac{T}{T_0} \tag{3}$$

The equation of continuity for water is

$$\frac{\partial(ud)}{\partial x}+\frac{\partial(vd)}{\partial y}=0 \tag{4}$$

The continuity equation for two-dimensional gas flow is

$$\frac{\partial(u\rho)}{\partial x}+\frac{\partial(v\rho)}{\partial y}=0 \tag{5}$$

From equations (4) and (5), a further condition for the analogy may be derived

$$\frac{d}{d_0}=\frac{\rho}{\rho_0} \tag{6}$$

Since for adiabatic isentropic flow in the gas

$$\frac{\rho}{\rho_0}=\left(\frac{T}{T_0}\right)^{\frac{1}{\gamma-1}} \tag{7}$$

and since, in the analogy, from equations (3) and (6)

$$\frac{\rho}{\rho_0}=\frac{d}{d_0}=\frac{T}{T_0}$$

then

$$\frac{T}{T_0}=\left(\frac{T}{T_0}\right)^{\frac{1}{\gamma-1}}$$

and, therefore, the analogy requires that $\gamma=2.0$

From the relation

$$\frac{p}{p_0}=\left(\frac{\rho}{\rho_0}\right)^{\gamma}$$

it may be seen, since $\gamma=2.0$, that

$$\frac{p}{p_0}=\left(\frac{d}{d_0}\right)^2 \tag{8}$$

The velocity potential for water is given by the equation

$$\phi_{xx}\left(1-\frac{\phi_x^2}{gd}\right)+\phi_{yy}\left(1-\frac{\phi_y^2}{gd}\right)-2\phi_{xy}\frac{\phi_x\phi_y}{gd}=0 \tag{9}$$

and the corresponding equation for a gas is

$$\phi_{xx}\left(1-\frac{\phi_x^2}{a^2}\right)+\phi_{yy}\left(1-\frac{\phi_y^2}{a^2}\right)-2\phi_{xy}\frac{\phi_x\phi_y}{a^2}=0 \tag{10}$$

Therefore, for identical expressions,

$$\frac{gd}{2gd_0}=\frac{a^2}{2gh_0} \tag{11}$$

From equations (9) and (10), the velocity $\sqrt{gd}$ in the liquid flow is seen to correspond to the velocity of sound in gas flow. In a subsequent section entitled "Discussion," the value of $\sqrt{gd}$ is shown to be the velocity of propagation of surface waves, the wave lengths of which are large in comparison with the water depth. The ratio of $V/\sqrt{gd}$ in the liquid flow corresponds to the Mach number V/a in the gas flow.

If the velocity of the liquid flow is less than $\sqrt{gd}$ ($M<1$), the water is said to be "streaming." If the velocity of liquid flow is greater than $\sqrt{gd}$ ($M>1$), the water is said to be "shooting."

In shooting water under certain conditions, the velocity of the flow may strongly decrease for short distances and the depth may increase. An unsteady motion of this type is called a hydraulic jump. Hydraulic jumps of small intensity are propagated with the velocity $\sqrt{gd}$.

The analogy may be summarized as follows:

Significant quantities and characteristics of two-dimensional compressible gas flow, $\gamma=2$	Corresponding values in analogous liquid flow
Temperature ratio, T/T_0	Water-depth ratio, d/d_0
Density ratio, ρ/ρ_0	Water-depth ratio, d/d_0
Pressure ratio, p/p_0	Square of water-depth ratio, $(d/d_0)^2$
Velocity of sound, $a=\sqrt{\frac{\gamma p}{\rho}}$	Wave velocity, $\sqrt{gd}$
Mach number, V/a	Mach number, $V/\sqrt{gd}$
Subsonic flow	Streaming water
Supersonic flow	Shooting water
Shock wave	Hydraulic jump

The Mach numbers in the liquid flow may easily be computed. If equation (1a) is substituted in the expression for stream Mach number

$$M=\frac{V_s}{\sqrt{gd_s}}$$

the expression becomes

$$M=\left[\frac{2(d_0-d_s)}{d_s}\right]^{1/2} \tag{12a}$$

The points for $M=1$ are located where the depth is two-thirds of the total head, as is easily verified from equation (12a). The local Mach numbers are computed from

$$M_l=\left[\frac{2(d_0-d_l)}{d_l}\right]^{1/2} \tag{12b}$$

The pressure coefficient, a significant quantity in compressible gas flow, may be computed for liquid flow. If $\left(\frac{d_1}{d_2}\right)^2$ is substituted for $\frac{p_1}{p_2}$ in the expression for pressure coefficient

$$P=F_c\left(\frac{\frac{p_l}{p_s}-1}{\frac{p_0}{p_s}-1}\right)$$

the expression becomes

$$P=F_c\left[\frac{\left(\frac{d_l}{d_s}\right)^2-1}{\left(\frac{d_0}{d_s}\right)^2-1}\right] \tag{13}$$

For a compressible gas

$$F_c=\frac{2}{\gamma M_s^2}\left[\left(1+\frac{\gamma-1}{2}M_s^2\right)^{\frac{\gamma}{\gamma-1}}-1\right]$$

and with $\gamma=2.0$, as required by the hydraulic analogy, the compressibility factor is exactly

$$F_c=1+\frac{1}{4}M_s^2$$

When the analogy is applied to the study of air flow, accurate quantitative results will not be obtained because, for strict agreement between water flow and gas flow, γ must equal 2.0, whereas for air γ is 1.4. The relation between pressure ratio and local Mach number for the two values of γ is shown in figure 1. A given pressure ratio corresponds to a higher Mach number in air than in the fictitious gas with $\gamma=2.0$. The corresponding depth ratios d/d_0 shown in figure 1 are equal to the square root of the pressure ratios for $\gamma=2.0$. With a given stream Mach number, the value of the critical negative-pressure coefficient (fig. 2) is greater in air than in the gas with $\gamma=2.0$. The differences are not very large, however, and the flow phenomena observed in the water flow should be qualitatively the same as those occurring in the two-dimensional compressible flow of air.

APPARATUS

The tests were conducted in the vertical, return-flow water channel which was designed and constructed in the

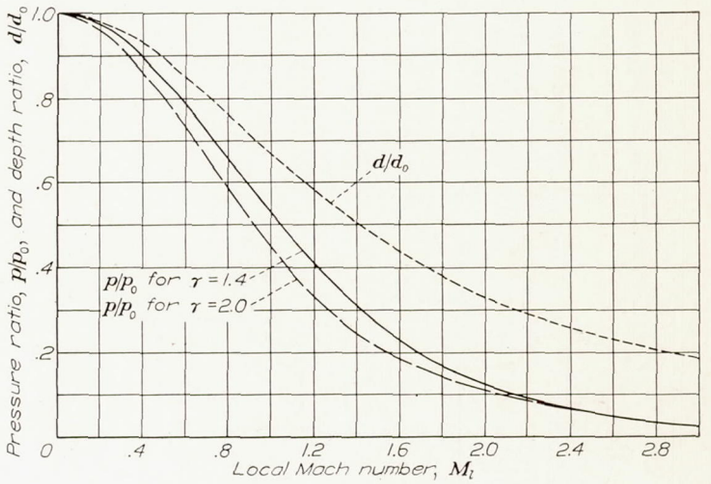


FIGURE 1.—Variation with local Mach number of pressure ratio p/p_0 in a compressible gas, and the water-depth ratio d/d_0 in the hydraulic analogy corresponding to $\sqrt{p/p_0}$ for $\gamma=2.0$.

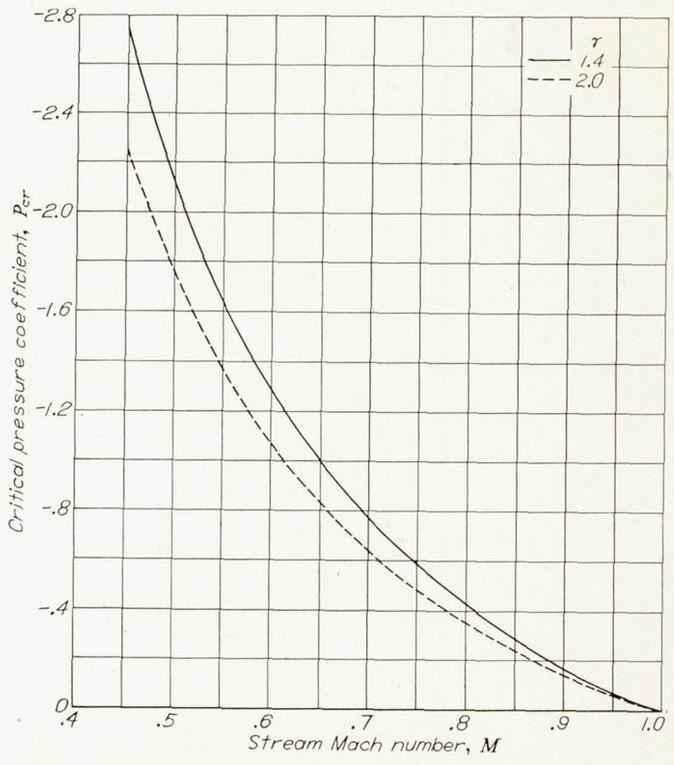
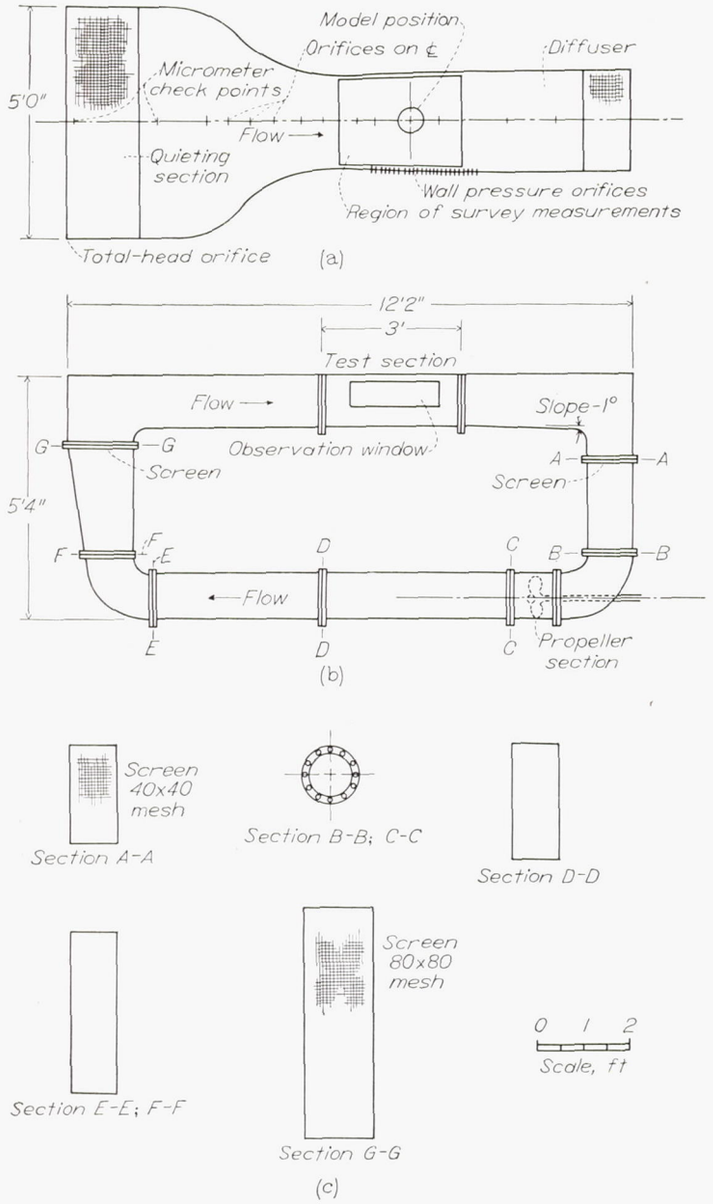


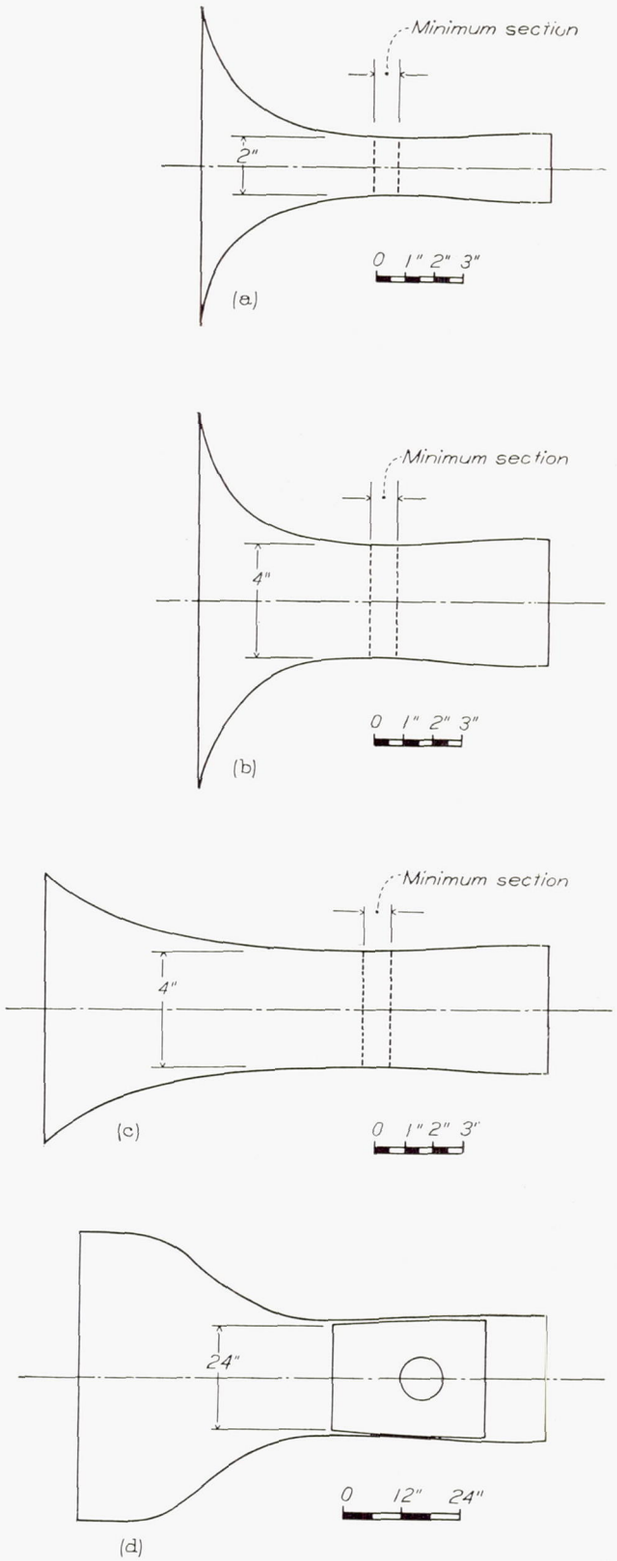
FIGURE 2.—Variation of critical pressure coefficient with Mach number.

Langley 8-foot high-speed tunnel. Figure 3 shows the flow circuit and plan view of the free water surface and also the orifice locations of the water channel. A motor-driven propeller of 1-foot diameter forces the water into the expanding section and through a screen into a large quieting section. The fluid is accelerated in the convergent section and flows through the test section downstream to the propeller so that continuous flow is maintained. The test section could be replaced by the nozzles shown in figures 4 (a) to 4 (c). The shape of the channel test section is given for comparison in figure 4 (d). The entire floor of the entrance cone and test section is horizontal except for the diffuser which has a 1° slope. For a static depth of 1.5 inches, the maximum volume flow is approximately 540 cubic inches per second and the power required is 1/10 horsepower.



(a) Plan view.
(b) Elevation.
(c) Cross sections.

FIGURE 3.—Schematic view of water channel with sections.



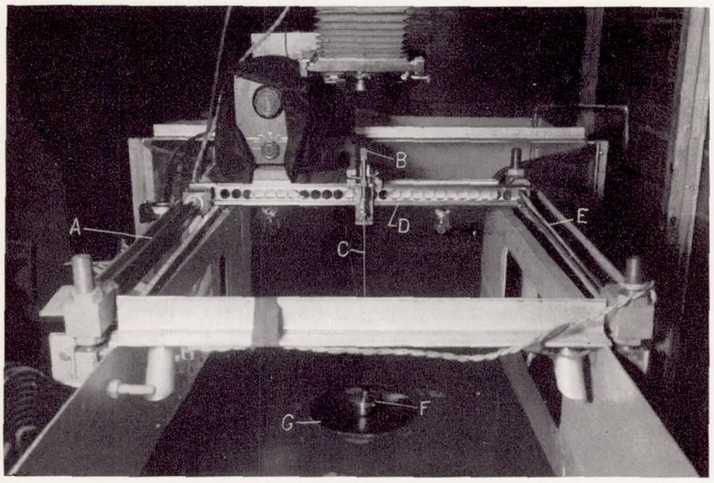
(a) Two-inch Laval nozzle (reference 4).
(b) Four-inch Laval nozzle (reference 4).
(c) Four-inch Laval nozzle with modified approach.
(d) Twenty-four-inch nozzle, final wall shape.

FIGURE 4.—Nozzle shapes for depth-ratio flow tests.

Water depths at points in the test section were obtained with the survey equipment shown in figures 5 and 6. A block on which was mounted a vertical shaft tipped with a fine wire probe (0.030-inch diameter) could be moved both parallel and perpendicular to the channel axis. The probe was capable of 2½-inch vertical travel continuously measurable by a standard micrometer to the nearest one-half thousandth of an inch. A small neon lamp was mounted in series with the insulated probe and the water to provide a positive sign of contact between the probe and water level.

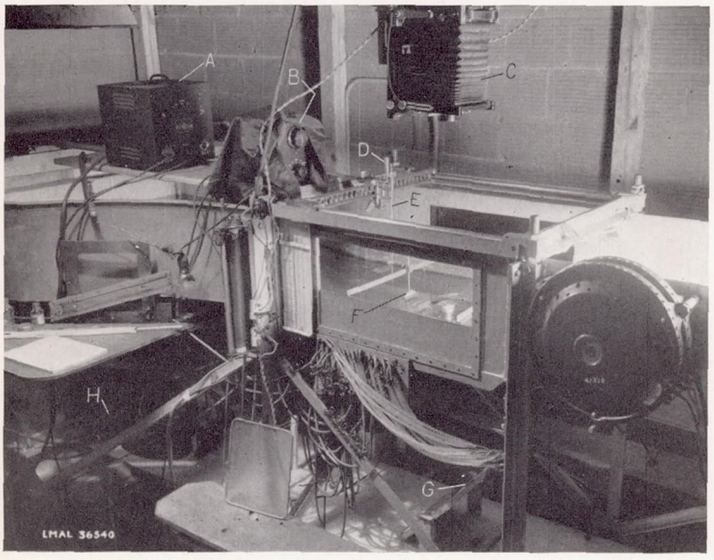
A similar micrometer unit, movable along a single fixed rail, was located upstream along the floor center line to measure total head. Water depths could also be measured by static orifices on the channel walls and along the floor. Each orifice was connected by a valve to a common sump and burette. By opening only one valve at a time, individual pressures could be obtained in the burette by means of a vernier height gage fitted with a hairline mirror sight. The locations of these orifices are shown in figure 3.

Photographs and motion pictures of the free surface could be obtained by cameras mounted above the test section. A Strobolux and Strobotac were used as the source of illumination. A circular glass plate, fitted into the center of the floor of the test section, permitted illumination of the water surfaces from below.



A Longitudinal rail
B Micrometer head
C Survey probe
D Cross rail
E Longitudinal rail
F Model
G Glass plate

FIGURE 5.—*Test section and survey equipment seen from downstream end of channel.*



A Strobolux
B Strobotac
C Camera
D Micrometer head
E Survey probe
F Support for ground-glass screen
G Mirror
H Position of light source

FIGURE 6.—Approach and test section showing equipment for photography.

METHODS

The two-dimensional models were mounted at the center of the glass plate, one end flush with the plate and the other end extending above the water surface. Orifices were drilled in the model a fixed distance above the glass plate and normal to the model surface.

From the theory of the hydraulic analogy, it is readily seen that accurate measurements must be made of the depths in all measurable points in the channel. For each operating speed two readings were usually obtained for each datum point, one by the burette and the other by the survey carriage. The burette reading, by means of the hairline sight and vernier, could be taken as quickly or as often as necessary without affecting stream conditions; whereas, because of the formation of capillary and standing waves, the surface probe reading was good only at the instant the probe touched the water. This effect was not serious at local supersonic speeds inasmuch as the standing waves were then unable to move upstream from the point of water contact. When the disturbance was removed by breaking contact with the water surface, original stream conditions were restored in about 10 seconds, at which time another reading could be made.

The micrometer unit movable along a single fixed rail measured the depth at the upstream positions and the depths at the first pressure orifice on the channel center line. From continuity considerations, the total head

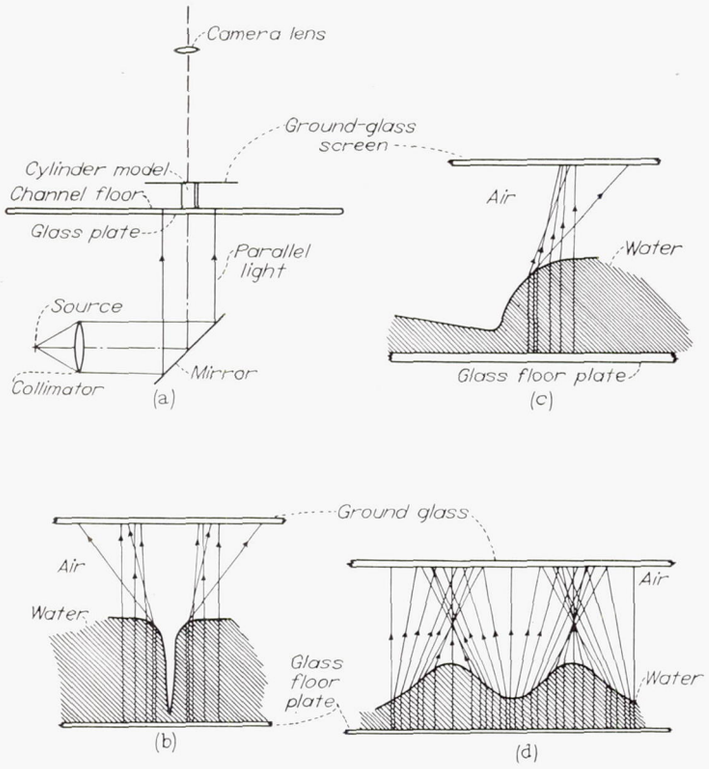
$$d_0 = d_s + \frac{d_1 - d_s}{1 - \left(\frac{d_s}{d_1}\right)^2 \left(\frac{b_s}{b_1}\right)^2} \tag{14}$$

where b is the breadth of the channel and subscript 1 refers to the station at the first orifice on the center line. The stream depth d_s was measured sufficiently far ahead in the test section to be unaffected by the presence of the model. The total head, however, could be measured directly by the upstream micrometer in the vicinity of the boundary wall at the upstream end (fig. 3). The upstream micrometer was calibrated against the test-section survey probe before each run. All depths were measured from the level floor of the channel. The net accuracy of all readings was within ± 0.002 inch.

Orifice pressures were used to obtain the water depth on the surface of the models and at the test-section side walls.

This type of measurement is necessary inasmuch as the capillary rise of water on all bodies that break the water surface invalidates the use of the survey probe. The probe is of great value, however, in obtaining surveys at points where the influence of capillarity is negligible, which in most cases is about ¼ inch from an exposed surface. Extreme care had to be taken in all pressure measurements to hold capillary rise constant in the burette, inasmuch as very slight concentrations of dirt on the glass would change the meniscus shape. The burette was, therefore, cleaned at regular intervals with chromic acid, and a 10-percent solution of aerosol was placed on the meniscus to reduce surface tension and capillarity. This procedure enabled consistent readings within the desired accuracy.

The shadowgraph still photographs were obtained by a 5- by 7-inch view camera. The test setup and schematic diagram are shown in figures 6 and 7 (a). In the initial trials it was found that the most convenient light source, with existing collimator lenses, was a Strobolux-Strobotac unit; and by adjusting the flash frequency, various light intensities could be obtained. The refraction patterns formed by a vortex, hydraulic jump, and capillary wave are shown in figures 7 (b) to 7 (d); and from these patterns or combinations, a qualitative analysis of shadowgraphs may be made. In order to reduce excessive pattern refraction, the ground-glass screen was placed as close to the water surface as possible. Motion pictures of wake frequencies and alternate trailing vortices were obtained by the same methods with no great difficulty.



(a) Shadowgraph ray diagram.
(b) Vortex.
(c) Hydraulic jump.
(d) Capillary wave.

FIGURE 7.—Analysis of method for photographing free surface.

RESULTS

In order to ascertain the nature and the applicability to air flow of data obtained in the water channel, tests were made with flow through nozzles and about circular cylinders. These tests were run at various depths and Mach numbers and with models of various sizes in the channel. The results are first presented without discussion.

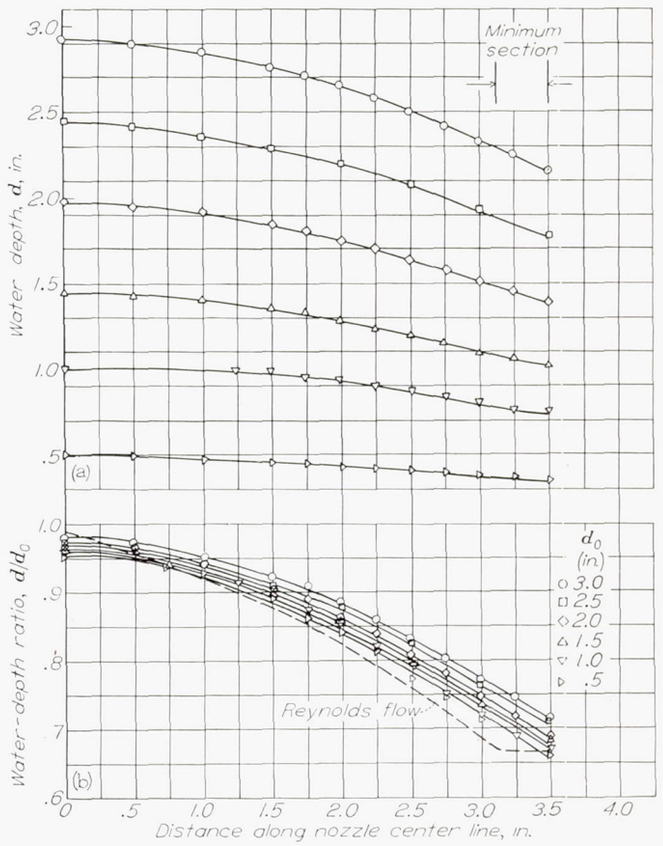
Plots of the water depths and water-depth ratios along the center line of convergent-divergent nozzles as measured by the test-section micrometer unit are shown in figures 8 to 10. The shapes of these nozzles are shown in figures 4 (a), 4 (b), and 4 (c), respectively. The curves labeled "Reynolds flow" are computed from one-dimensional theory; that is, the velocities at all points in a cross section are assumed the same in magnitude and parallel to the center line of the channel. The depth at any point is computed from the equation of continuity

$$V \times \text{Area} = \text{Constant} \tag{15}$$

where

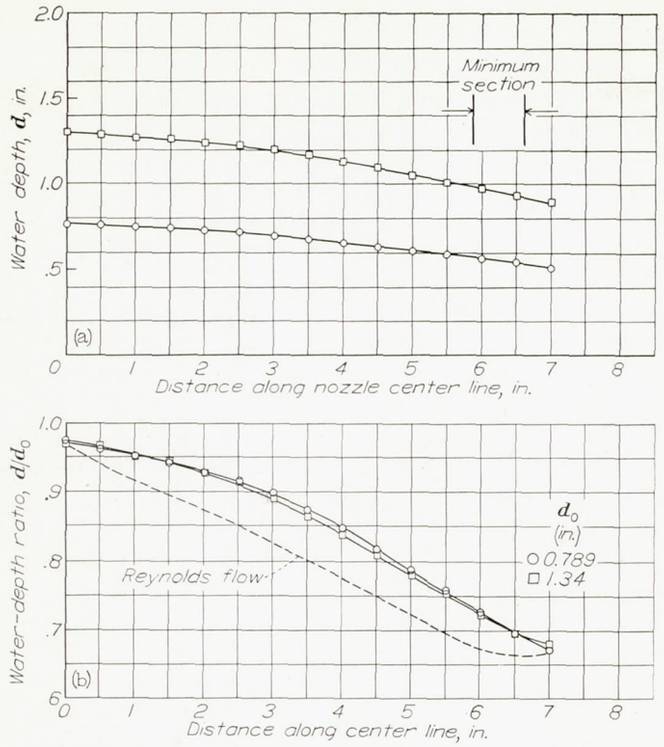
$$\text{Area} = \text{Breadth of the channel} \times \text{Water depth}$$

The water-depth ratios are seen to increase with the increase in depth in figure 8. The nozzle in figure 10 was modified to have a very gradual approach section and the water-depth ratios for this nozzle are the same at any depth.



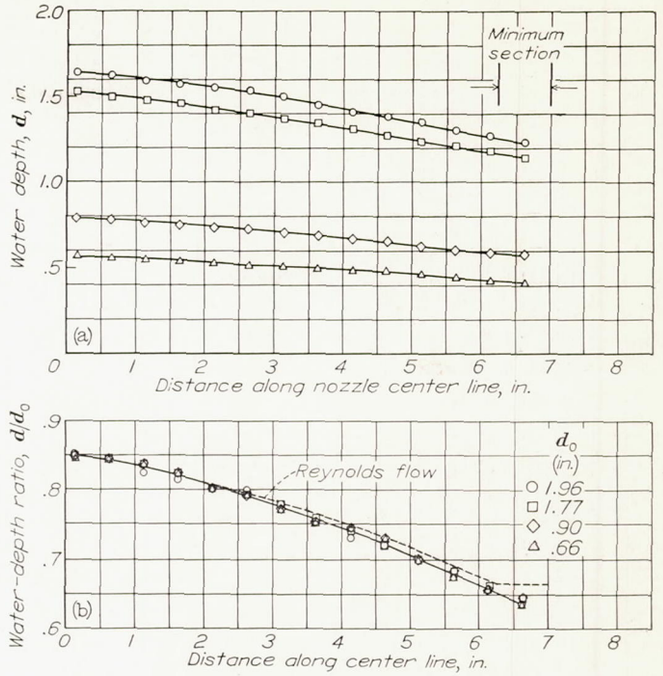
(a) Variation of water depth along center line showing shape of free surface.
(b) Variation of water-depth ratio d/d_0 along center line for different values of the total head d_0.

FIGURE 8.—Effect of change of total head on flow through a convergent-divergent nozzle. Throat width, 2 inches. Run at choking Mach number. Refer to figure 4 (a) for shape.



(a) Variation of water depth along center line showing shape of free surface.
(b) Variation of water-depth ratio d/d_0 along center line for different values of the total head d_0.

FIGURE 9.—Effect of change of total head on flow through a convergent-divergent nozzle. Throat width, 4 inches. Run at choking Mach number. Refer to figure 4 (b) for shape.



(a) Variation of water depth along center line showing shape of free surface.
(b) Variation of water-depth ratio d/d_0 along center line for different values of the total head d_0.

FIGURE 10.—Effect of change of total head on flow through a convergent-divergent nozzle. Throat width, 4 inches (modified approach section). Run at choking Mach number. Refer to figure 4 (c) for shape.

The variation with total head of the water depths and water-depth ratios about a circular cylinder as measured by means of the pressure orifices and burettes is shown in figure 11. In this case the depth ratios decrease with increase in water depth. A comparison between micrometer and burette measurements is shown for a 2-inch nozzle in figure 12, where it is seen that the micrometer readings are greater than the burette readings and the difference increases with depth.

Figures 13 and 14 show the variation with water depth of the shadowgraphs of the flow about a 2¼-inch-diameter circular cylinder at Mach numbers of 0.40 and 0.60, respectively. The corresponding variation of pressure at $\theta=90°$ is also shown. Additional shadowgraphs of the flow about circular cylinders of various sizes and with various water depths are shown in figures 15 to 19. The pressure distributions about the 2¼-inch circular cylinder in the water channel with a static depth of ¾ inch are compared for various Mach numbers in figure 20 with the pressure distributions about a ½-inch circular cylinder in air. The data for the circular cylinder in air were available from tests made in the Langley rectangular high-speed tunnel.

With various sizes of circular cylinders in the test section the variation of the local Mach numbers along the channel wall for different stream Mach numbers is shown in figures 21 to 24, and the corresponding stream depths d_s and total heads d_0 are given in figure 25.

DISCUSSION

Various factors influence the results obtained in the water channel, and the effect of these factors must be ascertained before the channel can be used for the investigation of the analogous gas flows.

From an examination of figures 15 to 19 it is seen that concentric waves appear in front of the model. The fact that these waves do not appear in the schlieren photographs (fig. 26) of air flow taken at the Langley rectangular high-speed tunnel suggests that these waves are not part of the analogy.

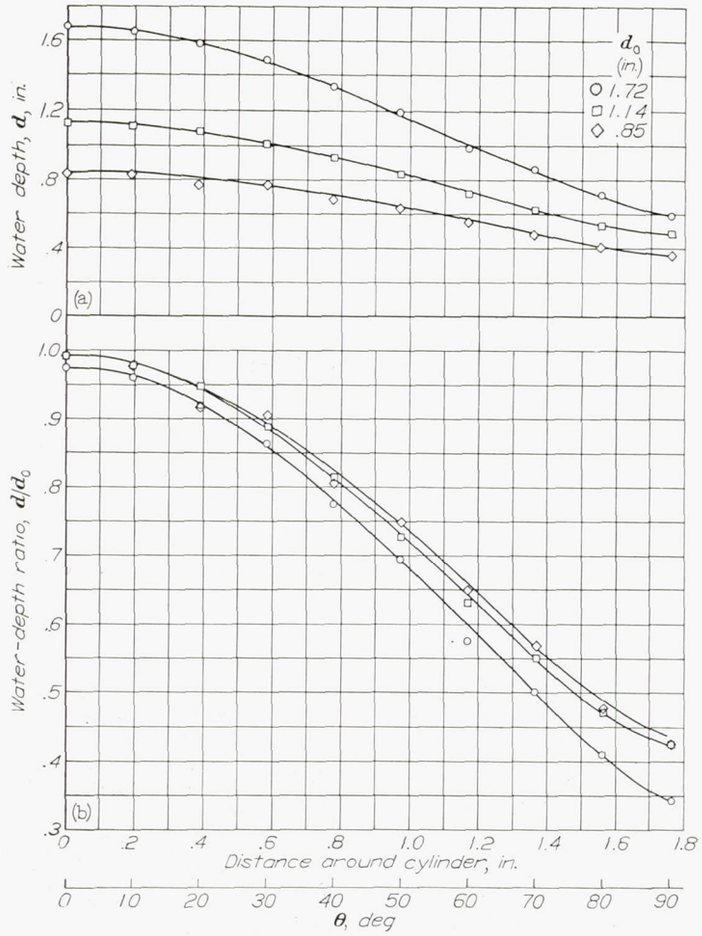
A disturbance at some point in a liquid generally will give rise to two types of waves—short surface-tension waves called capillary waves and considerably longer gravity waves (reference 5 and pp. 353–402 of reference 6). The expression for the velocity of propagation of water waves is

$$U=\left[\left(\frac{g\lambda}{2\pi}+\frac{2\pi\sigma}{\rho\lambda}\right)\tanh\frac{2\pi d}{\lambda}\right]^{1/2} \tag{16}$$

Figure 27 is a plot of U against λ for water depths of 0.5 inch and 2.0 inches. This figure shows that waves cannot exist with a velocity of propagation less than approximately 0.75 foot per second. Disturbances of wave length less than that corresponding to the minimum wave velocity are termed capillary waves since they depend primarily on the surface tension of the fluid. Propagation velocities greater than this minimum velocity correspond to shorter capillary waves and longer gravity waves.

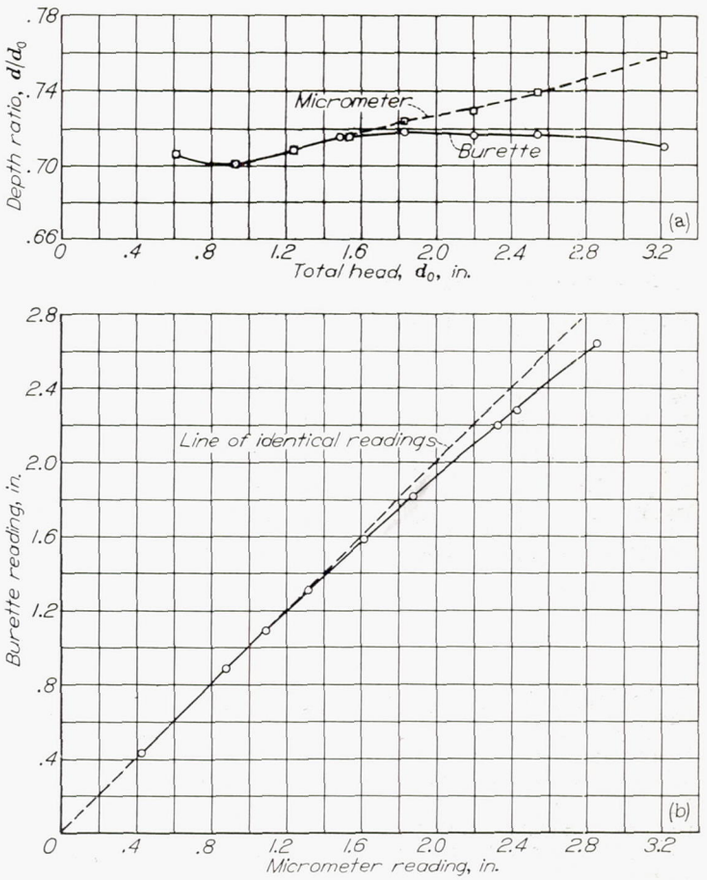
If $\sigma=0$ and $d\ll\lambda$, equation (16) becomes

$$U=\sqrt{gd} \tag{17}$$



(a) Water depths as determined by burette.
(b) Variation of water-depth ratio d/d_0 as determined by burette for different values of total head.

FIGURE 11.—Effect of change of total head on burette measurements at the surface of a 2¼-inch-diameter circular cylinder. $M=0.70$.



(a) Variation with total head d_0 of water-depth ratio measured by burette and micrometer.
(b) Comparison of micrometer and burette readings of depth.

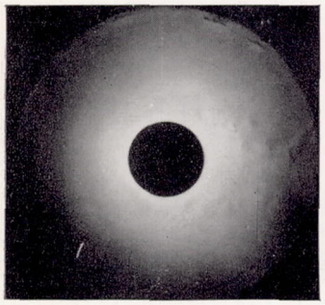
FIGURE 12.—Comparison of micrometer and burette measurements at the minimum section of the 2-inch nozzle.

and this velocity—the velocity of propagation of long gravity waves—is the basic surface wave velocity. The other waves defined by equation (16) are water surface waves and are not considered in the hydraulic analogy. Figure 27 shows that changes in the water depth have little effect on the velocity of propagation of waves for wave lengths less than 0.1 foot.

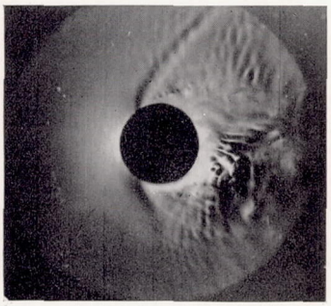
The wave lengths of some of the standing waves appearing in front of the models in figures 15 to 19 were measured from the photographs and were plotted in the inset of figure 27 against the local velocity (equal, for standing waves, to the velocity of propagation) at the point where the wave occurred. This plot showed that these waves were capillary waves. The check marks on the inset show the number of readings that fall on the plotted points. These capillary waves, although they have no part in the hydraulic analogy, have two adverse effects on the application of the analogy, namely, complication of the flow photographs and decrease in the accuracy of the depth measurements taken with the test-section probe.

The results obtained in the water channel depend to a large extent on the depth at which the tests are run. The effect of depth on the formation of standing capillary waves is shown in figure 28. If high stream Mach numbers without capillary waves in the stream are to be obtained, a shallow depth is prescribed.

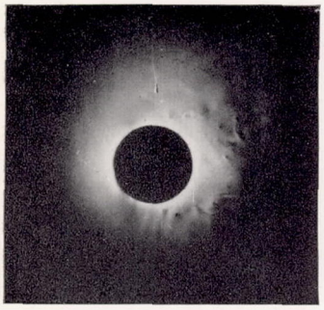
The effect of depth on the flow patterns and pressure coefficients about circular cylinders is very pronounced (figs. 13 and 14). The pressure coefficient rises to a maximum value at $d_{st}\approx 0.9$ inch. The decrease in pressure coefficient at lower depths is believed to be due to the effect of bottom boundary layer; the decrease at higher depths is due to the effect of the vertical accelerations. Comparison of figures 13 and 14 with figure 26 indicates that the water flow most nearly corresponds to air flow at depths that are between 0.75 inch and 1.0 inch.



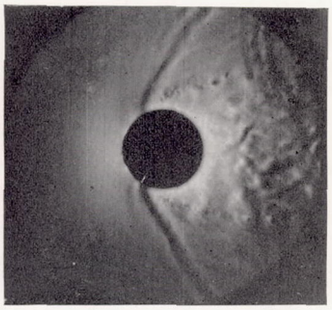
(a) d_{st}=0.50 inch.



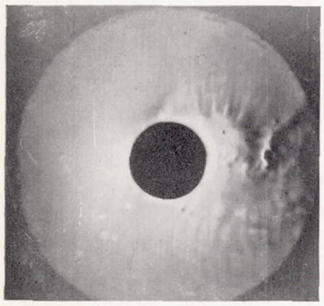
(d) d_{st}=1.50 inches.



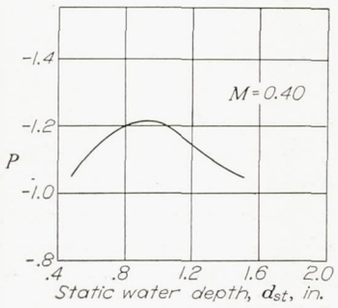
(b) d_{st}=0.75 inch.



(e) d_{st}=2.00 inches.

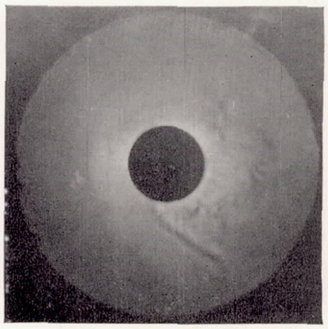


(c) d_{st}=1.00 inch.

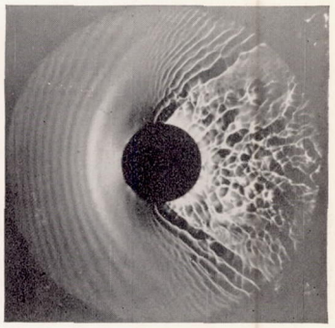


(f) Pressure coefficient, θ=90°.

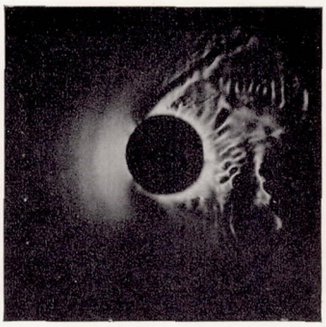
FIGURE 13.—Variation with static depth of flow pattern and pressure coefficient for the 2¼-inch-diameter circular cylinder. M=0.40.



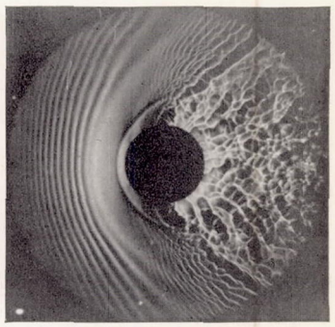
(a) d_{st}=0.50 inch.



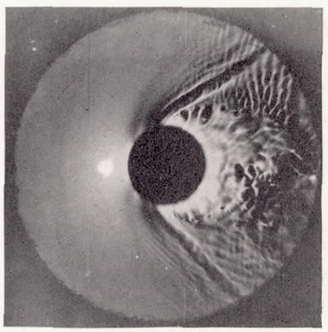
(d) d_{st}=1.50 inches.



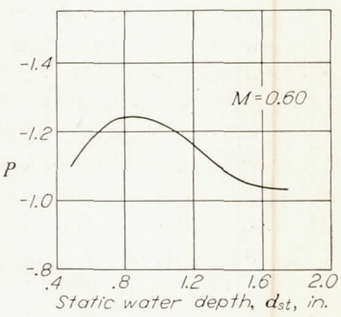
(b) d_{st}=0.75 inch.



(e) d_{st}=2.00 inches.

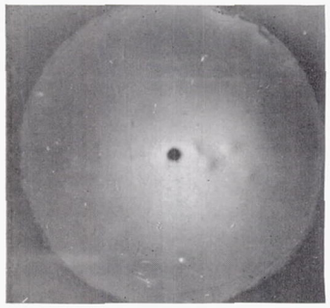


(c) d_{st}=1.00 inch.

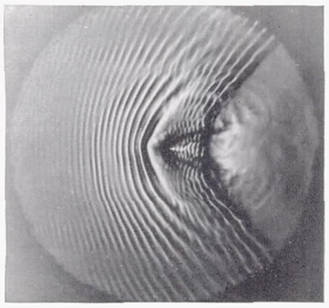


(f) Pressure coefficient, θ=90°.

FIGURE 14.—Variation with static depth of flow pattern and pressure coefficient for the 2¼-inch-diameter circular cylinder. M=0.60.



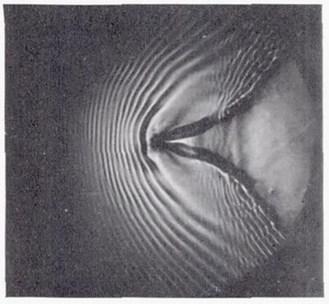
(a) $M=0.23$.



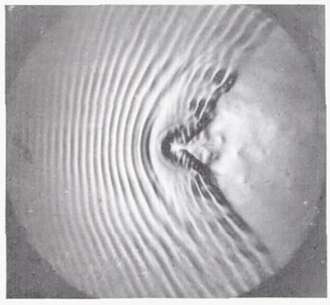
(d) $M=0.74$.



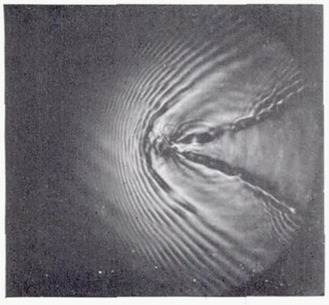
(b) $M=0.41$.



(e) $M=0.92$.

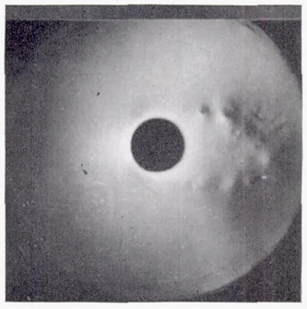


(c) $M=0.67$.

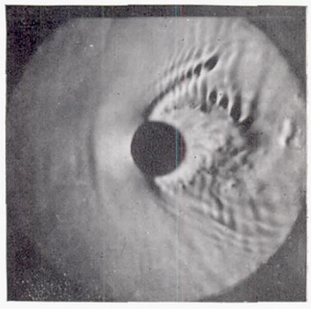


(f) $M=0.98$.

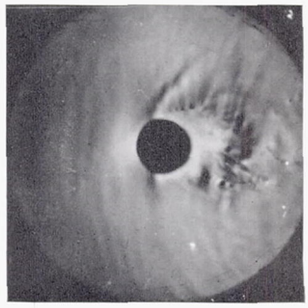
FIGURE 15.—Shadowgraphs of flow about the 0.30-inch-diameter circular cylinder. Static water depth, 1.00 inch.



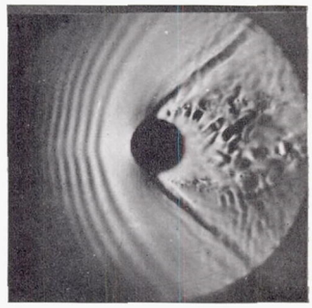
(a) $M=0.41$.



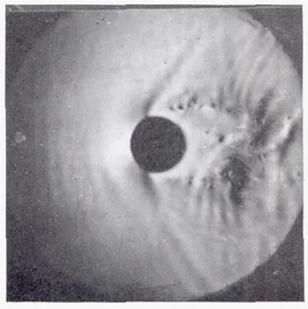
(d) $M=0.60$.



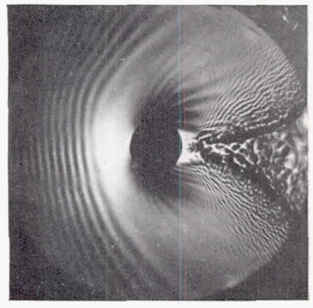
(b) $M=0.50$.



(e) $M=0.71$.

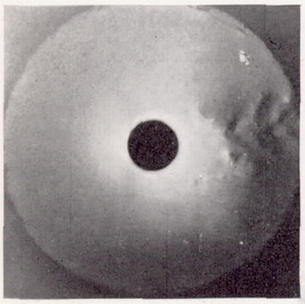


(c) $M=0.55$.

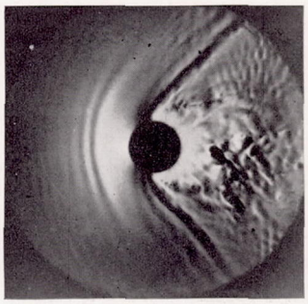


(f) $M=0.77$.

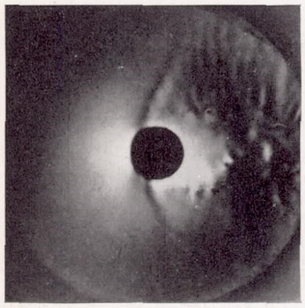
FIGURE 16.—Shadowgraphs of flow about the 1½-inch-diameter circular cylinder Static water depth, 0.76 inch.



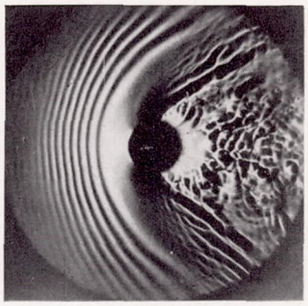
(a) M=0.34.



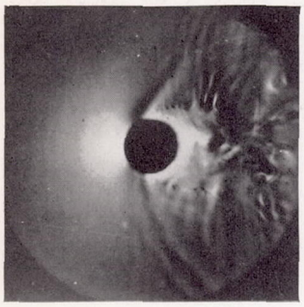
(d) M=0.60.



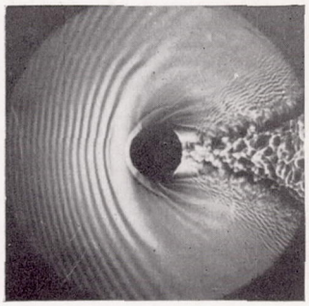
(b) M=0.46.



(e) M=0.72.

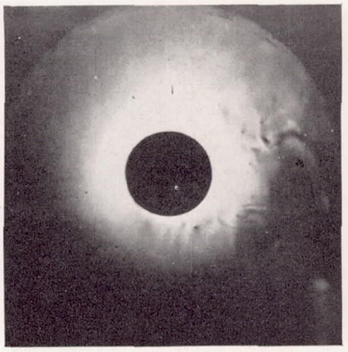


(c) M=0.50.

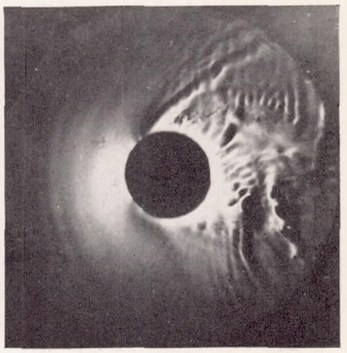


(f) M=0.78.

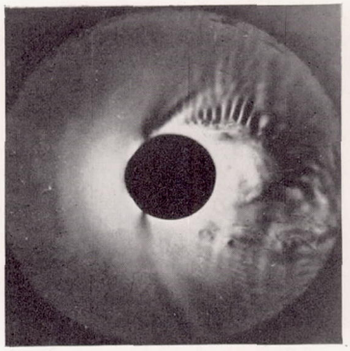
FIGURE 17.—Shadowgraphs of flow about the 1½-inch-diameter circular cylinder. Static water depth, 1.00 inch.



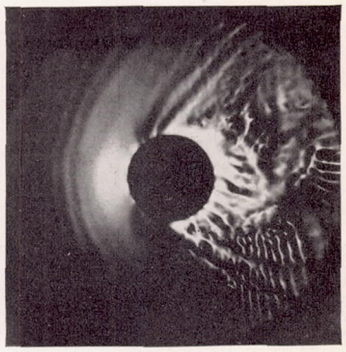
(a) M=0.41.



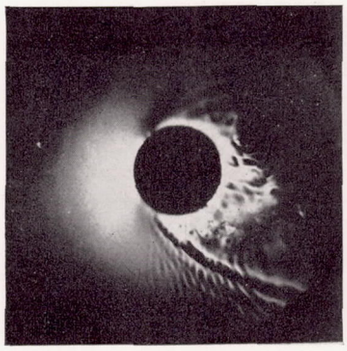
(d) M=0.61.



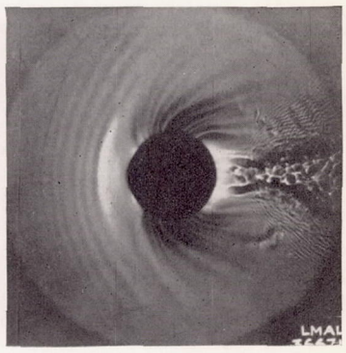
(b) M=0.51.



(e) M=0.65.

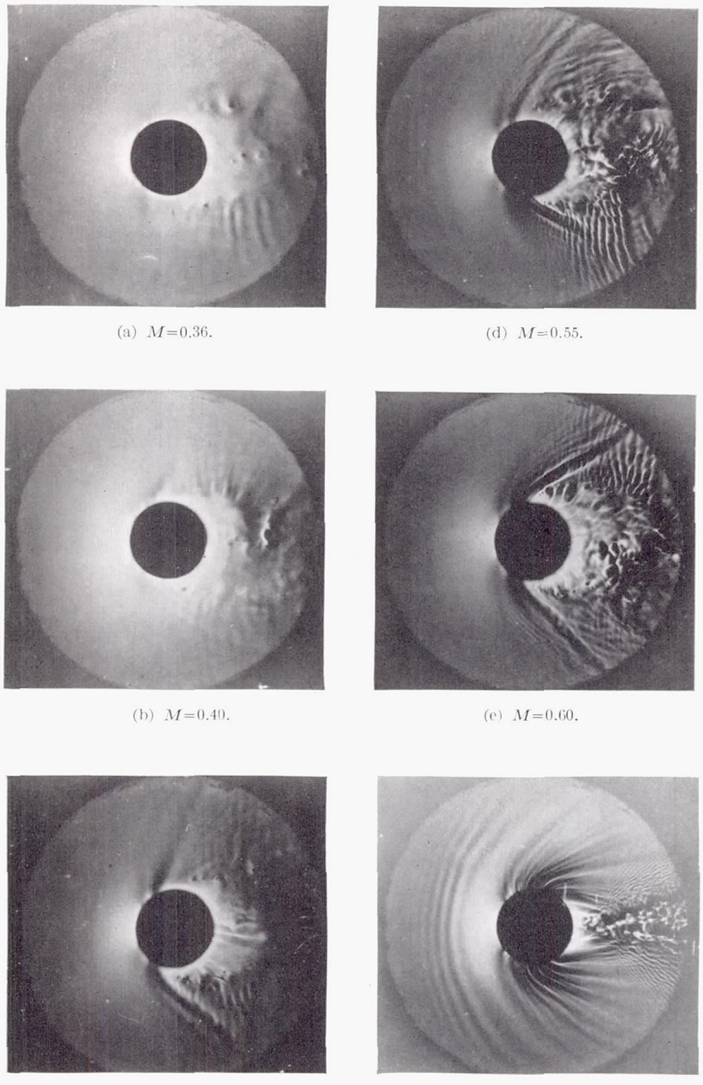


(c) M=0.55.



(f) M=0.71.

FIGURE 18.—Shadowgraphs of flow about the 2¼-inch-diameter circular cylinder. Static water depth, 0.75 inch.



(a) $M=0.36$. (d) $M=0.55$.

(b) $M=0.40$. (e) $M=0.60$.

(c) $M=0.49$. (f) $M=0.71$.

FIGURE 19.—Shadowgraphs of flow about the 2¼-inch-diameter circular cylinder. Static water depth, 1.00 inch.

The water is accelerated from the total head where the fluid velocity is zero to a value of zero acceleration and maximum velocity in the test section. The motion of the water through this cycle is actuated by the force of gravity which is thus the important factor in the hydraulic analogy. If an obstruction is placed in the path of a fluid at constant velocity, local accelerations of flow must take place in the field about the obstacle. If these accelerations are large, the vertical components, which have no part in the analogy, are no longer negligible in comparison with the acceleration of gravity; and a distortion of the flow results. This distortion is such that in a region of increasing deceleration, such as the region in which the flow is approaching stagnation, the depth is usually less than that required in the analogy; and the depth indicated by the pressure in the static orifices is greater than the true depth. In a region of increasing acceleration the opposite effects occur. The vertical acceleration depends upon the water depth and upon the slope and curvature of the free surface.

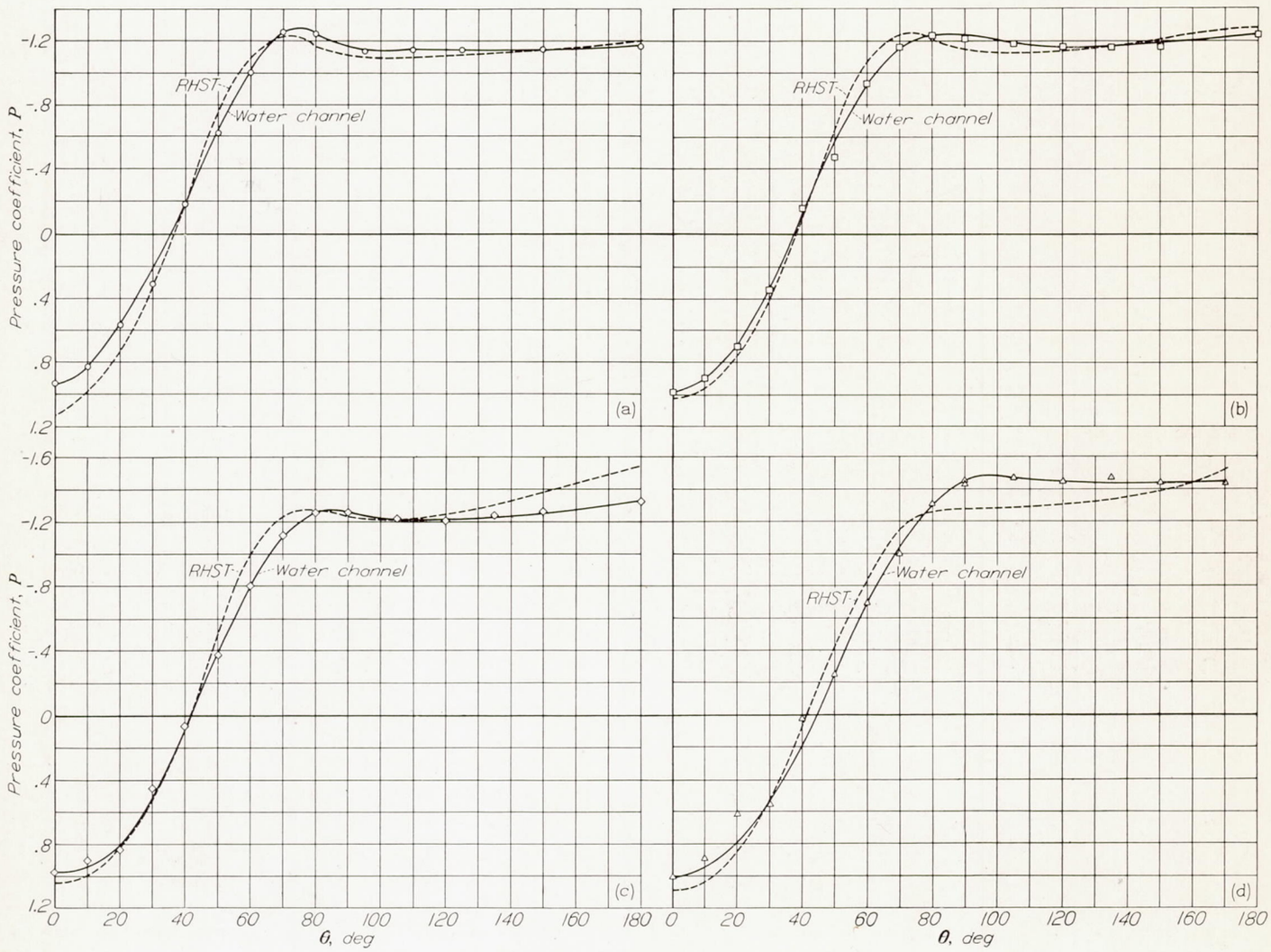
If the water depth is increased for two cases of the same stream Mach number, the slope and curvature of the free surface are likewise greater. This variation is shown in the following table in which the value of d_s is computed from equation (12a) for chosen values of M and d_0:

M	d_0	d_s	d_s/d_0	d_0-d_s	V (in./sec)
0.926	1.000	0.700	0.700	0.300	10.78
.926	1.100	.770	.700	.330	11.29

The slopes and curvatures of the free surface are approximately proportional to the term d_0-d_s, and the higher value of that term therefore corresponds in general to greater vertical accelerations. An illustration of the foregoing statements is given by the results of the nozzle tests in which, as the water depths decrease, the depth ratios approach those calculated by Reynolds flow (fig. 8); all tests were made at choking Mach number. Binnie and Hooker observed the same effect (reference 3). If the slope of the free surface is small and if the nozzle is so shaped that the acceleration in the entrance can be kept sufficiently small, no variation of water-depth ratios occurs with changing depth (fig. 10). The same effect is shown in figures 11 and 12 as measured by static orifices and burettes.

The effect of vertical accelerations on depth ratios determined by means of static orifices is opposite to that obtained by the probe. It may be assumed therefore that this adverse effect would be negligible when the two methods of reading pressures coincide. The readings taken at the minimum section of the 2-inch nozzle (fig. 12) coincided when the depth was reduced to 1.3 inches. If the free surface slope had been more abrupt (smaller model or model having a sharp pressure rise), a still shallower depth would have been required to attain this condition; therefore, large models and small depths should be employed. The minimum depth is limited, however, by the effects of the boundary layer on the floor of the channel.

The development of the boundary layer produces a velocity gradient along the channel similar to the gradient in a wind tunnel. This effect can be compensated in the same way by diverging the walls or in the case of the water channel by sloping the floor downward in the direction of flow. An effect for which compensation does not appear feasible is the thickening and thinning of the boundary layer in regions of decelerating and accelerating flow about a model, behavior which causes a distortion of the velocity distribution such as would correspond qualitatively to a thinning of the model. These boundary-layer effects are particularly serious in the water channel because of the appreciable boundary-layer displacement thickness (found to be of the order of 0.1 in.) in comparison with the total depth of the fluid. The boundary-layer effects could obviously be minimized by increasing the water depths, both because of the increased ratio of total depth to boundary-layer displacement thickness and because of the increased Reynolds numbers corresponding to the higher velocities with given Mach numbers. This requirement is, unfortunately, inconsistent with the minimizing of the effects of the capillary waves and of the vertical accelerations.



(a) M=0.41. (b) M=0.50.
(c) M=0.61. (d) M=0.71.

FIGURE 20.—Comparison of pressure distributions about a 2¼-inch circular cylinder in the water channel with the pressure distributions about a ½-inch circular cylinder in the Langley rectangular high-speed tunnel (RHST).

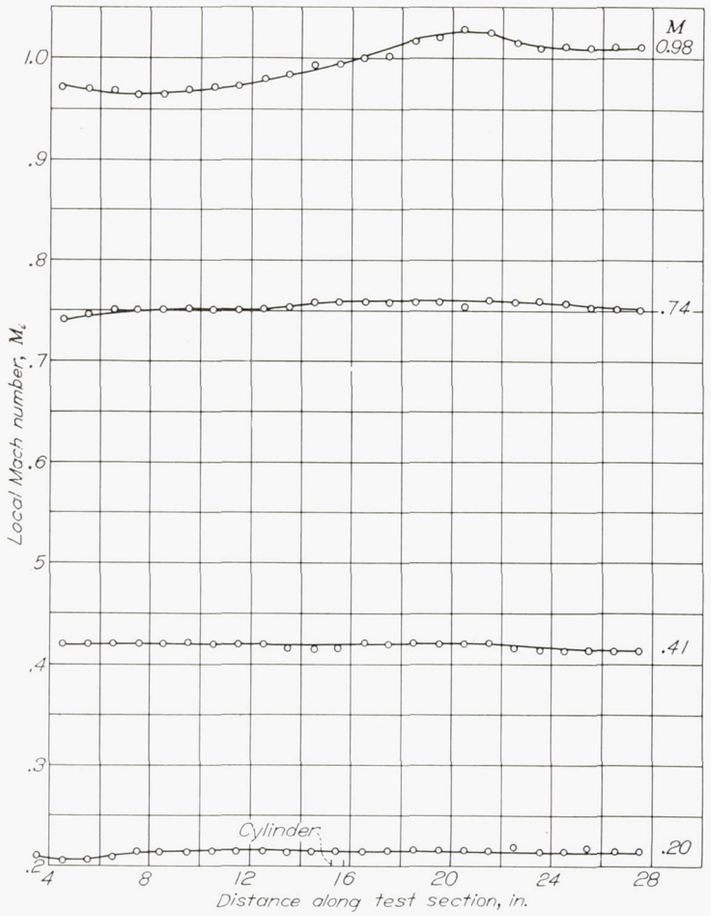


FIGURE 21.—Variation of local Mach number along channel wall with a 0.3-inch-diameter circular cylinder.

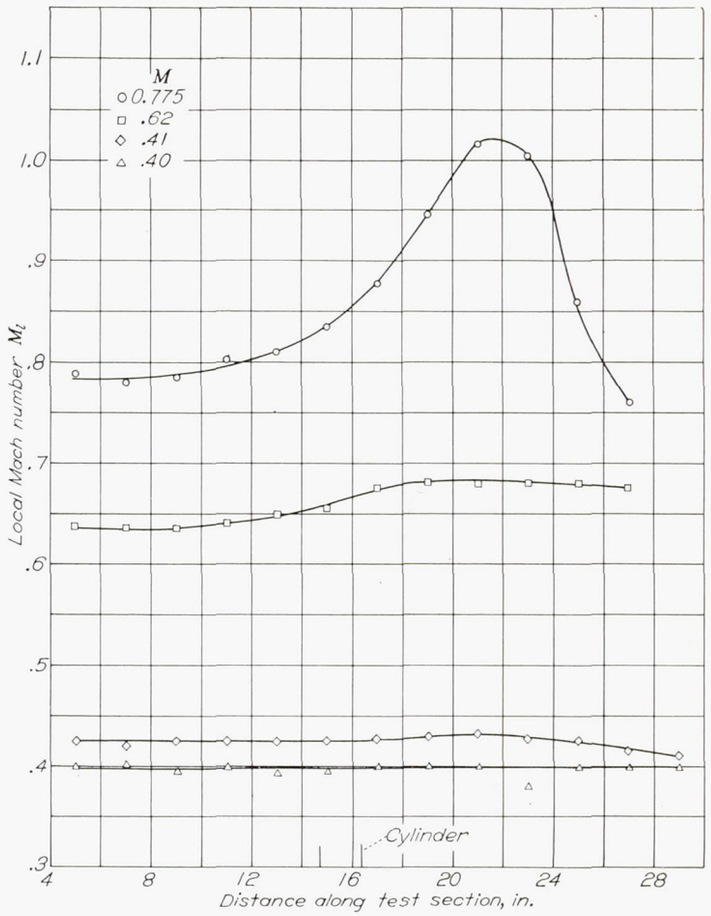


FIGURE 22.—Variation of local Mach number along channel wall with a 1½-inch-diameter circular cylinder.

The analogy is further limited by the fact that it applies for a hypothetical gas having a value of $\gamma=2.0$; the effect of this limitation has not been completely determined. The effects shown in figures 1 and 2 are not very large, however, and can be taken into account in the interpretation of data taken in the water channel. Other investigations suggest that the influence of the value of γ in subsonic compressible flow is not great. Kaplan (reference 7) thus found that to the third approximation the effect of the value of γ in the compressible flow up to the critical speed was negligible and Von Kármán (reference 8) obtained a widely used expression for change of pressure coefficient with Mach number by using the assumption $\gamma=-1$. For supersonic flow, the characteristics curves are considerably influenced by the value of γ. The ratio of maximum velocity to the velocity of sound is greater with $\gamma=1.4$ than with $\gamma=2.0$; and for a given change in flow angle, the velocity change, as determined by the characteristics method, is also greater.

The Reynolds numbers in the water channel are calculated for complete submersion and are very low; the maximum value of R for the 2¼-inch-diameter cylinder with a static water depth of 0.75 inch is 15,000. The comparison of the water-channel and wind-tunnel data (figs. 15 to 19 and 26) showed that, although the cylinder tests were made at considerably higher Reynolds numbers in air than in water, the same type of flow occurred in both cases; the main consideration is agreement of the flow patterns rather than identical Reynolds numbers.

In a wind tunnel, a choking or maximum stream Mach number occurs when local Mach numbers of 1.00 extend across the section between the model and tunnel walls. A similar effect was noted in the water channel. Figure 25 shows that the stream depth decreases and the total head increases with Mach number up to a maximum value that depends on the size of the model tested. At this choking condition, both the stream depth and the total head increase with an additional power input. Figure 29 shows the maximum Mach number for various ratios of cylinder diameter to channel width. Variation of the data from the theoretical curves might be expected inasmuch as the theoretical values were computed by one-dimensional theory (Reynolds flow); whereas, the actual flow is two-dimensional. Maximum Mach numbers that occur in wind tunnels, however, agree much more closely with the one-dimensional theory than do those shown in figure 29 (see reference 9); and it therefore seems likely that the divergence is due to other factors, such as boundary-layer effects and vertical accelerations, rather than to the two-dimensional nature of the flow.

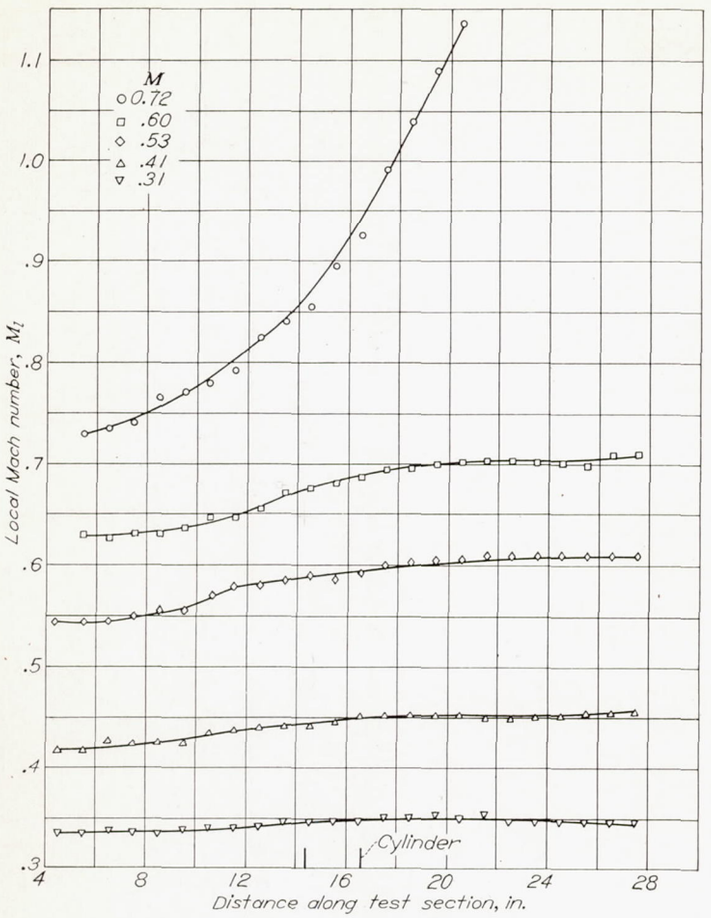


FIGURE 23.—Variation of local Mach number along channel wall with a 2¼-inch-diameter circular cylinder.

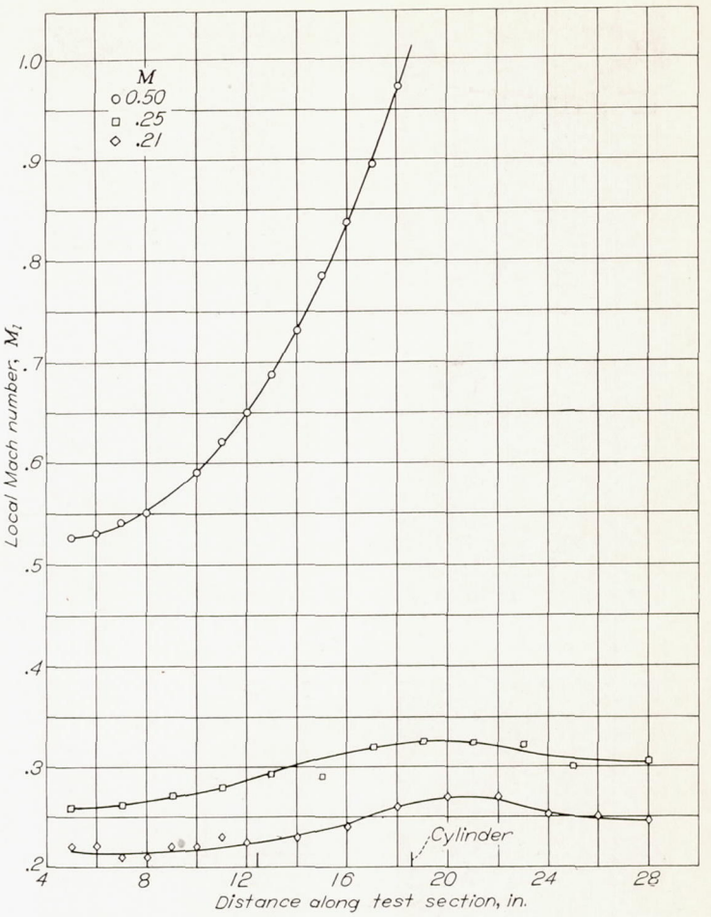


FIGURE 24.—Variation of local Mach number along channel wall with a 6-inch-diameter circular cylinder.

The disturbance along the channel wall with various size cylinders in the test section is shown in figures 21 to 24. The wall disturbance is an indication of the severity at high Mach numbers of channel-wall or wind-tunnel-wall interference. As the stream Mach number approaches 1.00, the wall disturbance increases until at the choking condition the interference becomes large even for the smallest cylinder. For the 1½-inch-diameter cylinder (fig. 22), the point of sonic velocity at the wall is located approximately 3 diameters behind the cylinder. This result is in agreement with the flow photographs (figs. 15 and 17), which show a gull-wing-shaped shock starting from the region behind the cylinder and extending downstream toward the walls. Figure 30 shows the lines of constant Mach number in the flow field about a 6-inch-diameter cylinder at choking Mach number and shows clearly the supersonic flow occurring behind the cylinder.

A comparison of the shadowgraphs (figs. 15 to 19) with schlieren photographs of flow about circular cylinders in air (fig. 26) shows that the two flows are very similar. The type of flow is the same in the two cases and is the type that is characteristic of Reynolds numbers somewhat below the critical value. At Reynolds numbers between 50 and 350,000, an unstable condition is set up behind a circular cylinder in which vortices are shed alternately from each side. Laminar separation occurs at a point approximately 80° from the forward stagnation point and a vortex sheet is formed which extends downstream and finally rolls up into a large vortex. The vortices so shed arrange themselves into a Kármán street. (See reference 6, pp. 217–218.)

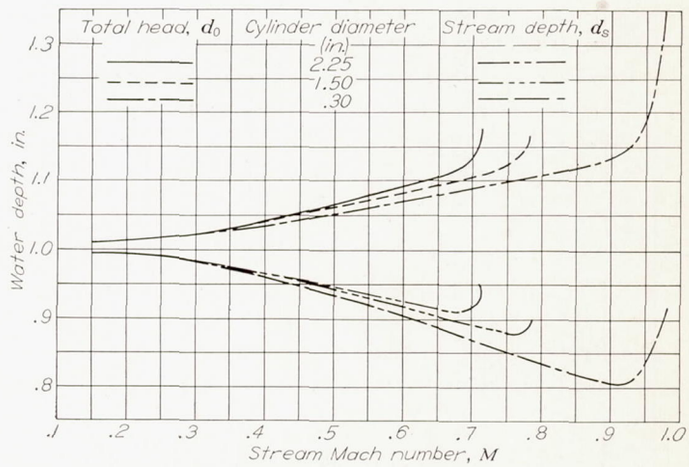
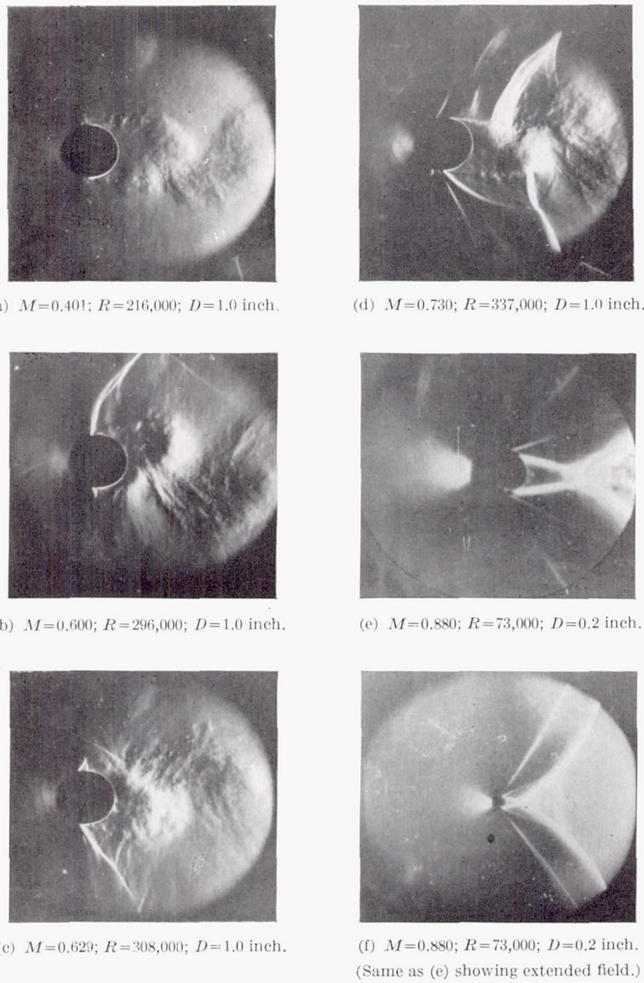


FIGURE 25.—Variation with stream Mach number of stream depth and total head with circular cylinders in the test section. d_{st}=1.00 inch.



(a) $M=0.401$; $R=216{,}000$; $D=1.0$ inch.

(d) $M=0.730$; $R=337{,}000$; $D=1.0$ inch.

(b) $M=0.600$; $R=296{,}000$; $D=1.0$ inch.

(e) $M=0.880$; $R=73{,}000$; $D=0.2$ inch.

(c) $M=0.629$; $R=308{,}000$; $D=1.0$ inch.

(f) $M=0.880$; $R=73{,}000$; $D=0.2$ inch. (Same as (e) showing extended field.)

FIGURE 26.—Schlieren photographs of circular cylinders in the Langley rectangular high-speed tunnel.

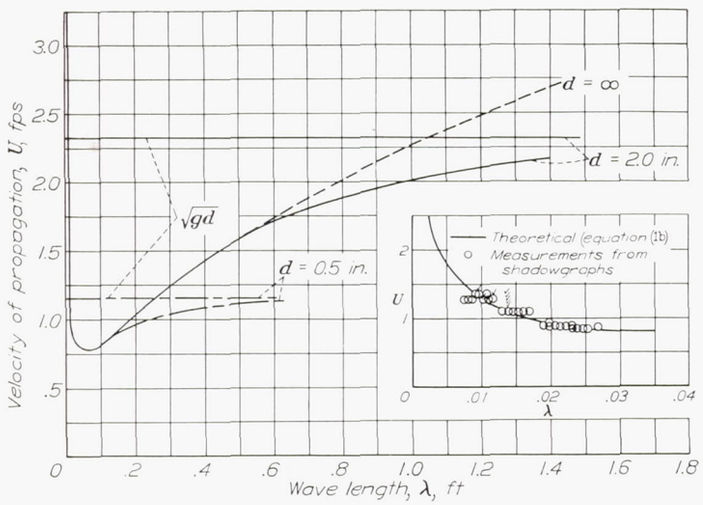


FIGURE 27.—Variation of velocity of propagation of water surface waves with wave length.

Figures 16 (a), 18 (a), 19 (b), and 26 (a) show this type of flow, which is the same in the water channel as in the air flow. Because of the occurrence of separation, the actual pressure distribution is different from that calculated by potential-flow theory. The actual pressures over the forward part of the cylinder are higher and those over the rear are lower than those calculated by theory. The negative pressure peak is greatly reduced. Figure 20 shows the pressure distributions about circular cylinders in air and in the water channel. The quantitative results obtained in the water channel are very close to those obtained in air (figs. 20 (a) to 20 (c)). This close agreement is believed, however, to be largely fortuitous, resulting from an interaction between the bottom-boundary-layer effects and the rather large channel-wall interference in the water channel. At the choking Mach number $M=0.71$ in the water channel (see fig. 20 (d)), the interference effects exceed the relieving effects of the thinning of the boundary layer, and the negative pressure coefficients near $\theta=90°$ exceed those obtained in the wind tunnel.

Because of the unsteady nature of the flow, instantaneous velocities greater than those indicated by the pressure distributions occur near the surface of a cylinder. The critical speed may therefore be expected to be lower than indicated by the pressure distributions, an effect that has been observed in air. Figure 2 shows that with a given peak negative pressure coefficient the critical Mach number should be somewhat lower in the water channel ($\gamma=2.0$) than in air ($\gamma=1.4$).

Another effect of the unsteady flow is the asymmetrical development of shock. When the flow closes in on one side of the cylinder, the induced velocities increase and the local Mach number may exceed 1.00. A shock wave may thus form on one side while none exists on the other or a more intense shock may exist on one side than on the other. Such asymmetrical shock patterns are shown in figures 16 (b) to 16 (d), 17 (b), 18 (b) to 18 (d), and 26 (b) to 26 (d). Exactly the same phenomenon occurs in the water channel as in the air flow. In some cases, the shedding of these waves alternately from each side of a cylinder has been observed in the water channel when the stream Mach number was only a little above the critical value. Such behavior is to be expected if on one side of the cylinder the velocities first exceed and then fall below the speed of sound as the flow closes in and then breaks away from the surface. With increase in Mach number, a strong disturbance originates at the edge of the wake approximately 1 diameter behind the cylinder and extends into the field of flow (figs. 15 (d), 18 (d), and 26 (d)). This disturbance oscillates with the wake, which is still unstable, and in its incipient stages alternates from one side of the model to the other. At still higher speed, the flow closes in behind the cylinder so that the cylinder has the appearance of a streamline body with a strong gull-wing-shaped disturbance at its trailing edge (figs. 15 (e), 15 (f), 16 (f), 17 (f), 18 (f), 19 (f), 26 (e), and 26 (f)). These features appear to be essentially the same in the water channel as in the air flow.

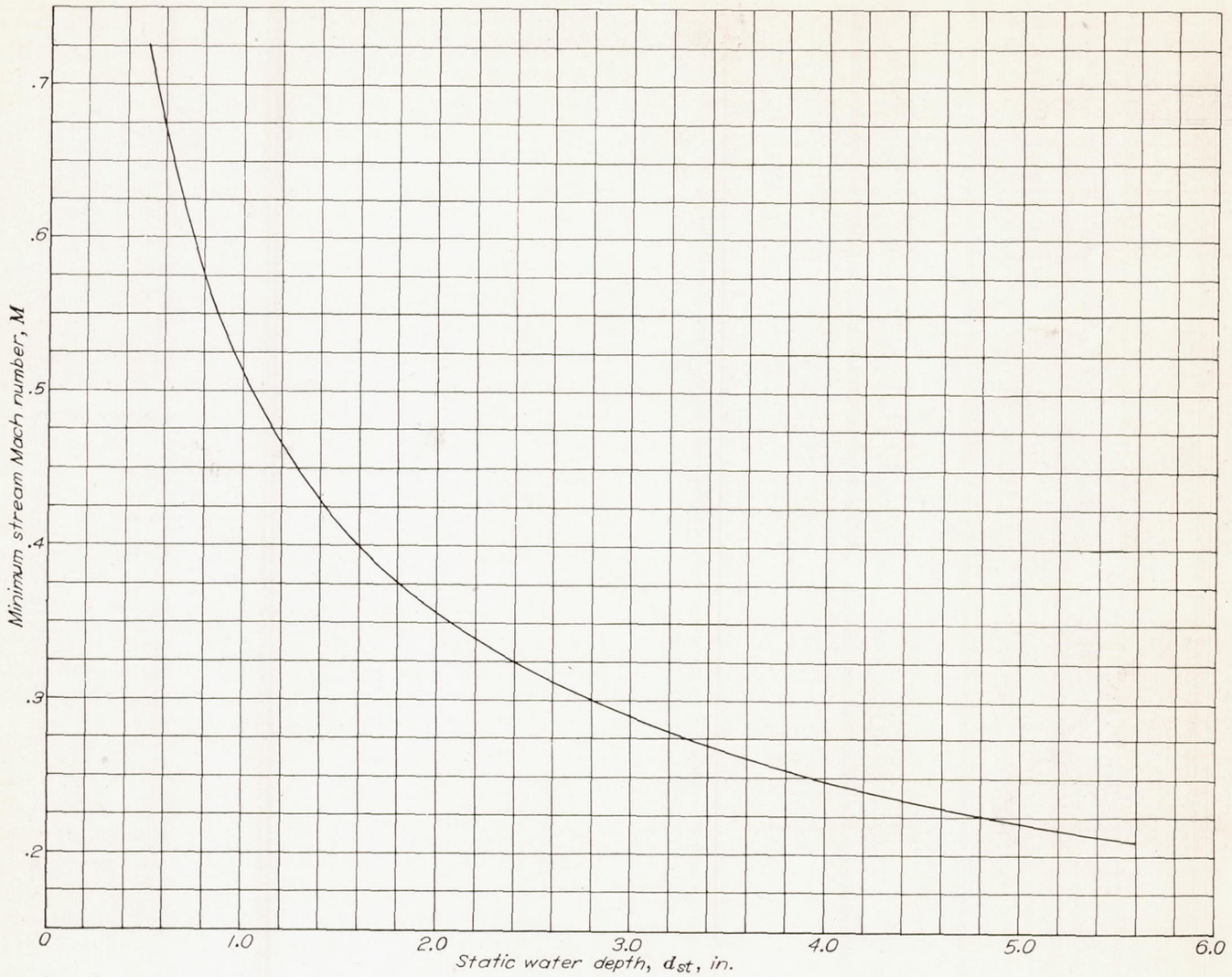


FIGURE 28.—Minimum stream Mach number at which standing capillary waves form in free stream.

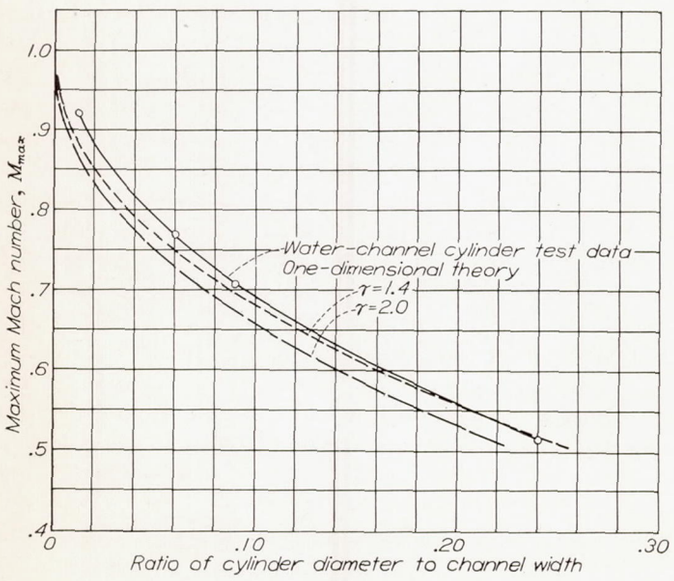


FIGURE 29.—Water-channel maximum test Mach number.

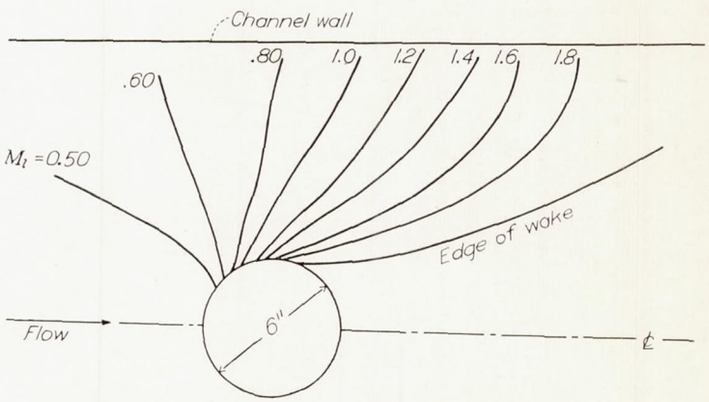


FIGURE 30.—Lines of constant Mach number in the flow field about a 6-inch-diameter circular cylinder in the 24-inch water channel at maximum stream Mach number. M=0.51.

EQUIPMENT AND FUTURE DEVELOPMENT

Measurement of depth at the surface of models and at fluid boundaries are best made with pressure orifices and burettes because of the capillary rise, whereas the micrometer method is suited for measurement of field depths; both methods agree very well provided the vertical accelerations are small. The burette method is best for obtaining average pressures in unstable flow. A method of photography has been developed that is simple and completely satisfactory. The shadowgraphs of the water flow are strikingly similar to the schlieren photographs of the air flow.

The value of the water channel lies mainly in the low cost and convenience of operation. Field surveys are simply made, and various features of the flow such as turbulence, vortices, separation, and shock formation are easily observed and photographed. Streamlines about a model are easily obtained by inserting streams of dye in the water ahead of the model.

A larger channel especially designed to minimize boundary-layer effects and to secure uniform flow in the test section is desirable. The channel should be large enough to permit tests at Reynolds numbers above the critical value. A larger channel would also be advantageous in reducing the adverse effects of the boundary layer or vertical accelerations, or both.

Additional investigations, both theoretical and experimental, are needed in order to determine the corrections necessary to convert quantities obtained from the water flow to the values characteristic of the air flow about corresponding bodies.

CONCLUSIONS

An experimental apparatus and technique have been developed for the investigation of the analogy between water flow with a free surface and two-dimensional compressible gas flow (hydraulic analogy); a preliminary investigation has been made and the results of an application of the analogy have been presented. The following conclusions are indicated from this work:

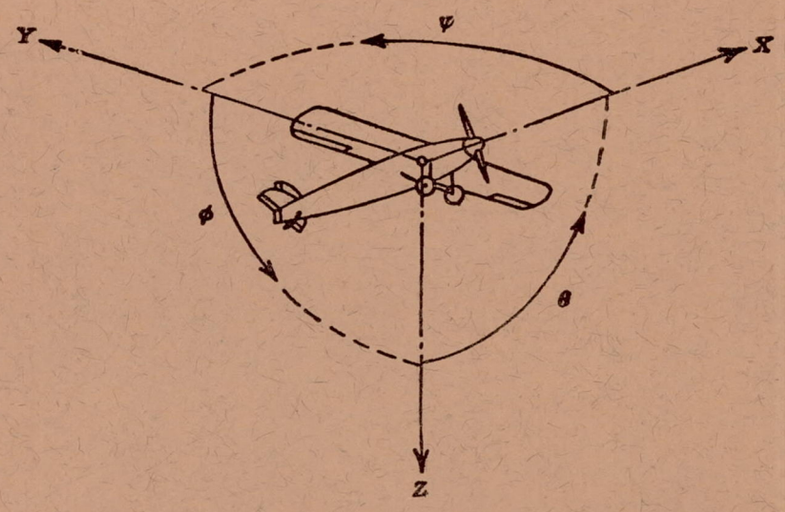
1. The hydraulic analogy provides a very inexpensive and convenient means of investigating high-speed two-dimensional air flow. The flow may be observed and photographed, and surface and field measurements may be easily obtained. Reasonably satisfactory agreement was found between the water flow and air flow about corresponding bodies, although considerable work in both theory and experiment is needed in order to convert with quantitative accuracy from the water flow to the flow in air.
2. With a larger channel, difficulties due to vertical accelerations and subcritical Reynolds numbers might be overcome.

LANGLEY MEMORIAL AERONAUTICAL LABORATORY,
NATIONAL ADVISORY COMMITTEE FOR AERONAUTICS,
LANGLEY FIELD, VA., *August 21, 1946.*

REFERENCES

1. Riabouchinsky, D.: Mécanique des fluides. Comptes Rendus, t. 195, no. 22, Nov. 28, 1932, pp. 998–999.
2. Riabouchinsky, Dimitri: Mécanique des fluides. Comptes Rendus, t. 199, no. 14, Oct. 1, 1934, pp. 632–634.
3. Binnie, A. M., and Hooker, S. G.: The Flow under Gravity of an Incompressible and Inviscid Fluid through a Constriction in a Horizontal Channel. Proc. Roy. Soc. (London), ser. A, vol. 159, no. 899, April 1937, pp. 592–608.
4. Preiswerk, Ernst: Application of the Methods of Gas Dynamics to Water Flows with Free Surface.
 Part I. Flows with No Energy Dissipation. NACA TM No. 934, 1940.
 Part II. Flows with Momentum Discontinuities (Hydraulic Jumps). NACA TM No. 935, 1940.
5. Page, Leigh: Introduction to Theoretical Physics. D. Van Nostrand Co., Inc., 1928, pp. 218–224.
6. Rouse, Hunter: Fluid Mechanics for Hydraulic Engineers. McGraw-Hill Book Co., Inc., 1938.
7. Kaplan, Carl: Two-Dimensional Subsonic Compressible Flow past Elliptic Cylinders. NACA Rep. No. 624, 1938.
8. Von Kármán, Th.: Compressibility Effects in Aerodynamics. Jour. Aero. Sci., vol. 8, no. 9, July 1941, pp. 337–356.
9. Byrne, Robert W.: Experimental Constriction Effects in High-Speed Wind Tunnels. NACA ACR No. L4L07a, 1944.

U. S. GOVERNMENT PRINTING OFFICE: 1949



Positive directions of axes and angles (forces and moments) are shown by arrows

Axis		Force (parallel to axis) symbol	Moment about axis			Angle		Velocities	
Designation	Symbol		Designation	Symbol	Positive direction	Designation	Symbol	Linear (component along axis)	Angular
Longitudinal	X	X	Rolling	L	$Y \longrightarrow Z$	Roll	ϕ	u	p
Lateral	Y	Y	Pitching	M	$Z \longrightarrow X$	Pitch	θ	v	q
Normal	Z	Z	Yawing	N	$X \longrightarrow Y$	Yaw	ψ	w	r

Absolute coefficients of moment

$C_l = \frac{L}{qbS}$ (rolling) $\quad C_m = \frac{M}{qcS}$ (pitching) $\quad C_n = \frac{N}{qbS}$ (yawing)

Angle of set of control surface (relative to neutral position), δ. (Indicate surface by proper subscript.)

4. PROPELLER SYMBOLS

D Diameter

p Geometric pitch

p/D Pitch ratio

V' Inflow velocity

V_s Slipstream velocity

T Thrust, absolute coefficient $C_T = \frac{T}{\rho n^2 D^4}$

Q Torque, absolute coefficient $C_Q = \frac{Q}{\rho n^2 D^5}$

P Power, absolute coefficient $C_P = \frac{P}{\rho n^3 D^5}$

C_s Speed-power coefficient $= \sqrt[5]{\frac{\rho V^5}{P n^2}}$

η Efficiency

n Revolutions per second, rps

Φ Effective helix angle $= \tan^{-1}\left(\frac{V}{2\pi r n}\right)$

5. NUMERICAL RELATIONS

1 hp = 76.04 kg-m/s = 550 ft-lb/sec

1 metric horsepower = 0.9863 hp

1 mph = 0.4470 mps

1 mps = 2.2369 mph

1 lb = 0.4536 kg

1 kg = 2.2046 lb

1 mi = 1,609.35 m = 5,280 ft

1 m = 3.2808 ft